

Geochemistry, Geophysics, Geosystems

RESEARCH ARTICLE

10.1029/2021GC009657

Key Points:

- Alkenone carbon isotope fractionation primarily influenced by CO₂, cell size, and irradiance, with a smaller effect from growth rate
- Diffusive model, the basis for conventional alkenone paleobarometer, of carbon isotope fractionation does not describe culture data
- Irradiance is necessary to accurately describe alkenone carbon isotope fractionation and should be considered in the natural environment

Supporting Information:

Supporting Information may be found in the online version of this article.

Correspondence to:

S. R. Phelps,
sphelps@fas.harvard.edu

Citation:


Phelps, S. R., Hennon, G. M. M., Dyhrman, S. T., Hernández Limón, M. D., Williamson, O. M., & Polissar, P. J. (2021). Carbon isotope fractionation in Noelaerhabdaceae algae in culture and a critical evaluation of the alkenone paleobarometer. *Geochemistry, Geophysics, Geosystems*, 22, e2021GC009657. <https://doi.org/10.1029/2021GC009657>

Received 15 JAN 2021

Accepted 28 MAY 2021

© 2021. American Geophysical Union.
All Rights Reserved.

Carbon Isotope Fractionation in Noelaerhabdaceae Algae in Culture and a Critical Evaluation of the Alkenone Paleobarometer

Samuel R. Phelps^{1,3} , Gwenn M. M. Hennon^{2,4} , Sonya T. Dyhrman^{1,2},
Maria D. Hernández Limón^{1,5} , Olivia M. Williamson^{2,6} , and Pratigya J. Polissar^{2,7} 

¹Department of Earth and Environmental Sciences, Columbia University, New York, NY, USA, ²Division of Biology and Paleo-Environment, Lamont-Doherty Earth Observatory of Columbia University, Palisades, NY, USA, ³Now at Department of Earth and Planetary Sciences, Harvard University, Cambridge, MA, USA, ⁴Now at College of Fisheries and Ocean Sciences, University of Alaska Fairbanks, Fairbanks, AK, USA, ⁵Now at Department of the Geophysical Sciences, University of Chicago, Chicago, IL, USA, ⁶Now at Rosenstiel School of Marine and Atmospheric Science, University of Miami, Miami, FL, USA, ⁷Now at Department of Ocean Sciences, University of Santa Cruz, Santa Cruz, CA, USA

Abstract The carbon isotope fractionation in algal organic matter (ϵ_p), including the long-chain alkenones produced by the coccolithophorid family Noelaerhabdaceae, is used to reconstruct past atmospheric CO₂ levels. The conventional proxy linearly relates ϵ_p to changes in cellular carbon demand relative to diffusive CO₂ supply, with larger ϵ_p values occurring at lower carbon demand relative to supply (i.e., abundant CO₂). However, the response of *Gephyrocapsa oceanica*, one of the dominant alkenone producers of the last few million years, has not been studied closely. Here, we subject *G. oceanica* to various CO₂ levels by increasing pCO₂ in the culture headspace, as opposed to increasing dissolved inorganic carbon (DIC) and alkalinity concentrations at constant pH. We note no substantial change in physiology, but observe an increase in ϵ_p as carbon demand relative to supply decreases, consistent with DIC manipulations. We compile existing Noelaerhabdaceae ϵ_p data and show that the diffusive model poorly describes the data. A meta-analysis of individual treatments (unique combinations of lab, strain, and light conditions) shows that the slope of the ϵ_p response depends on the light conditions and range of carbon demand relative to CO₂ supply in the treatment, which is incompatible with the diffusive model. We model ϵ_p as a multilinear function of key physiological and environmental variables and find that both photoperiod duration and light intensity are critical parameters, in addition to CO₂ and cell size. While alkenone carbon isotope ratios indeed record CO₂ information, irradiance and other factors are also necessary to properly describe alkenone ϵ_p .

1. Introduction

Anthropogenic CO₂ emissions are perturbing the global carbon cycle more rapidly than at any time in the last 66 million years (Zeebe et al., 2016). A key component of the natural carbon cycle is coccolithophores, which modify oceanic dissolved inorganic carbon and alkalinity inventories through photosynthetic carbon fixation and the biogenic production of calcium carbonate plates (Balch et al., 1992). These eukaryotic algae are abundant and widely distributed throughout the global oceans today (Geitzenauer et al., 1976; Hagino & Young, 2015; McIntyre & Bé, 2003) and in Cenozoic sediments (Burky, 1971; Gartner, 1969). Certain coccolithophores in the family Noelaerhabdaceae—such as *Emiliania huxleyi* and *Gephyrocapsa oceanica* (Young et al., 2003)—are well known for the long-chain unsaturated ketone molecules they produce (Marlowe et al., 1984). These lipid biomarkers, called alkenones, have been found in sediments as old as 120 Ma (Brassell & Dumitrescu, 2004) and can easily be isolated from sediments and other co-occurring organic compounds. Because alkenones are produced only by the Noelaerhabdaceae, the carbon isotope ratios of these molecules ($\delta^{13}\text{C}_{\text{Mk}37:2}$) have been used to estimate atmospheric CO₂ concentrations over the last ~45 Ma (e.g., Jasper and Hayes, 1990; Jasper et al., 1994; Pagani et al., 1999, 2005).

The carbon stable isotope fractionation recorded in algal organic matter has been used for decades as a CO₂ paleobarometer (Freeman & Hayes, 1992; Popp et al., 1989). The carboxylating enzyme Ribulose 1, 5-bisphosphate carboxylase/oxygenase (RuBisCO) in plants and algae prefers ¹²C to ¹³C by ~11–30 %, depending

on the specific form of RuBisCO employed by the organism (Boller et al., 2011, 2015; Falkowski & Raven, 2007; Goericke et al., 1994). This kinetic preference makes photosynthetic particulate organic carbon ($\delta^{13}\text{C}_{\text{POC}}$) depleted in ^{13}C relative to the ambient aqueous CO_2 ($\delta^{13}\text{C}_{\text{CO}_2\text{aq}}$). The carbon isotope fractionation is termed ϵ_p and is calculated using Equation 1.

$$\epsilon_p = \left(\delta^{13}\text{C}_{\text{CO}_2\text{aq}} + 1 \right) / \left(\delta^{13}\text{C}_{\text{POC}} + 1 \right) - 1 \quad (1)$$

The magnitude of carbon isotope fractionation during photosynthesis (ϵ_p) has been found to be inversely related to the ambient $\text{CO}_{2(\text{aq})}$ concentration. All else constant, as $[\text{CO}_{2(\text{aq})}]$ declines, so too does the diffusive influx of CO_2 , reducing the apparent carbon isotope fractionation in organic matter relative to the external CO_2 source (Rau et al., 1989, 1992). In addition to $[\text{CO}_{2(\text{aq})}]$, culture experiments have identified other environmental and physiological factors that influence algal $\delta^{13}\text{C}$ values, including algal growth rate, species, and growth conditions, such as irradiance or nutrient limitation (Burkhardt et al., 1999; Laws et al., 1995; Riebesell, Burkhardt, et al., 2000; Rost et al., 2002; Thompson & Calvert, 1995).

The original framework for interpreting alkenone $\delta^{13}\text{C}$ values was modified from a model of carbon isotope fractionation in plants (Farquhar et al., 1982), and was formulated with cellular CO_2 supply only by passive diffusion. In this framework, ϵ_p values are linearly related to the ratio of cellular carbon demand to diffusive CO_2 supply. Throughout this paper, the term “diffusive model” refers to this quantitative framework of the alkenone- CO_2 proxy, as formalized by Rau et al. (1996). Many studies have considered how non-diffusive CO_2 supply affects the carbon isotope ratio of DIC entering the cell and the resulting ϵ_p values (Badger, 2021; Franco et al., 1993; Freeman & Pagani, 2005; Laws et al., 1997; 2002; Pagani, 2014; Rau et al., 2001; Stoll et al., 2019). However, the majority of alkenone ϵ_p records to date have been interpreted using the diffusive model (Badger et al., 2019; Bae et al., 2015; Pagani et al., 1999, 2011; Zhang et al., 2013, 2017, 2019, 2020). Furthermore, many studies have used this framework to account for cell size changes, using scaling factors that are predicated on diffusive supply (Badger et al., 2019; Henderiks & Pagani, 2007; Popp, Laws, et al., 1998; Zhang et al., 2017, 2020).

The application of the diffusive model is undermined by evidence for pervasive non-diffusive CO_2 supply in algae (Bach et al., 2013; Badger et al., 1998; Beardall & Raven, 2013; Laws et al., 2002; Rost et al., 2003; Stojkovic et al., 2013) and recent measurements of much smaller kinetic fractionation by RuBisCO in *E. huxleyi* (Boller et al., 2011). Non-diffusive CO_2 supply in algae counteracts photorespiration (Andersson, 2008), carbon limitation at $[\text{CO}_{2(\text{aq})}]$ levels found in many parts of the ocean (Heureux et al., 2017; Olsen et al., 2016; Young et al., 2016), and the requirement by RuBisCO of an additional CO_2 molecule to activate the enzyme (Andersson, 2008; Lorimer & Miziorko, 1980). Non-diffusive supply through carbon concentrating mechanisms (CCMs) is not included in the diffusive model and will change the relationship between ϵ_p and carbon demand/supply (Freeman & Pagani, 2005; Laws et al., 1997, 2002).

Recent direct measurement of the carbon isotope fractionation by RuBisCO in *E. huxleyi* presents a further challenge to the diffusive model. For conventional alkenone paleobarometry applications, the maximum possible ϵ_p is set by the kinetic fractionation by RuBisCO (termed ϵ_f in the diffusive model). Based upon the value of RuBisCO (form IB) fractionation in higher plants (Goericke et al., 1994; O’Leary, 1984; Roeske & O’Leary, 1985) and inference from algal cultures (Popp, Laws, et al., 1998), a value of $\sim 25\text{‰}$ is used for RuBisCO form ID (the form found in alkenone-producing coccolithophores). However, in vitro measurements of RuBisCO extracted from *E. huxleyi* yielded $\epsilon_{\text{RuBisCO}} = 11.1\text{‰}$ (95% CI: 9.8–12.6‰) (Boller et al., 2011). Here, “ ϵ_f ” denotes the maximum fractionation in vivo, and $\epsilon_{\text{RuBisCO}}$ denotes the measured fractionation in vitro (Wilkes & Pearson, 2019). This low $\epsilon_{\text{RuBisCO}}$ value suggests that other fractionating mechanisms must generate ^{13}C -depleted CO_2 at the site of carboxylation to allow ϵ_p to exceed $\epsilon_{\text{RuBisCO}}$. Wilkes and Pearson (2019) proposed a photocatalytic CCM that is capable of explaining the discrepancy between the measured in vitro RuBisCO fractionation and the inferred in vivo value of 25‰. The hypothesized pathway is enhanced under excess photon flux and involves hydroxylation of CO_2 to HCO_3^- during DIC transfer across the thylakoid membrane, then conversion of HCO_3^- to CO_2 to be used for carbon fixation. This process is proposed to produce highly ^{13}C -depleted CO_2 surrounding RuBisCO and ϵ_p values that approach ϵ_f (25‰). This and other studies have identified an influence of environment on ϵ_p that is independent of carbon demand

and diffusive CO₂ supply, which needs to be considered when attempting to use algal ϵ_p as a paleobarometer (Holtz et al., 2017; Rost et al., 2002; Stoll et al., 2019; Wilkes & Pearson, 2019).

Here, we report new measurements of carbon isotope fractionation (ϵ_p) in *G. oceanica* in response to variable [CO_{2(aq)}] achieved through pCO₂ headspace manipulation, the first investigation of the photosynthetic carbon isotope response of this alga to modified pH. We compile and carefully standardize published datasets to probe the relationship between ϵ_p and carbon demand relative to diffusive CO₂ supply. We evaluate the results in the framework of the diffusive model that has been used to infer past CO₂ levels. We find that more of the variance in ϵ_p can be explained by the light conditions in cultures than by the diffusive model. We show that accounting for both irradiance and photoperiod is necessary to describe photosynthetic carbon isotope fractionation in alkenone-producing algae in culture, and suggest irradiance is likely a key variable in the natural environment.

2. Methods

2.1. *G. Oceanica* Cultures

2.1.1. Culture Set-Up

We grew non-axenic batch cultures of *G. oceanica* (Roscoff Culture Collection RCC1303; isolated from the Bay of Biscay in 1999) in triplicate at five different CO₂ partial pressures, with target pCO₂ of 200, 400, 600, 800, and 1000 μatm . Cultures were conducted simultaneously, and the stock strain was pre-acclimated to each CO₂ level for ~ 5 generations prior to the experimental treatment. The experimental design followed Hennon et al. (2019). CO₂ concentrations were set in 2.5-L polycarbonate culture flasks (filled with 1 L of media) by continuously aerating the headspace of the bottle with gas from tanks with $\sim 79\%$ N₂, 21% O₂, and either 200, 400, 600, 800, or 1000 ppmv CO₂ (acquired from TechAir, NY, USA). Culture media were not bubbled because this has been shown to have adverse effects on the physiology of algal cultures (Juhl & Latz, 2002). Instead, gas streams of pre-mixed CO₂ partial pressures were directed through sterilized glass pipets and positioned just above the media surface to break the boundary layer, thereby the [CO_{2(aq)}] of each vessel was set by diffusion from the headspace. The gas stream tubing was held in place above the headspace-media interface by wrapping the tubing in cheesecloth and wedging the cheesecloth between the tubing and the mouth of the polycarbonate vessel. Cells were grown in 0.2- μm filtered natural seawater collected from Avery Point, CT, USA. Nutrients were based on the L1 recipe (Guillard & Hargraves, 1993) but reduced as follows: L1/15 phosphate, L1/10 nitrate, and L1/25 vitamins and trace metals. The salinity was 32.53, and cultures were incubated at 18°C. Light intensity was measured using a QSPL-2100 light meter (Biospherical Instruments Inc., San Diego, CA, USA) and was delivered in a 14:10 photoperiod (light on from 08:00 to 22:00 h). Light intensity in the culture chamber varied slightly depending on flask location but averaged $99 \pm 14 \mu\text{mol photons m}^{-2} \text{ s}^{-1}$ (mean and one standard deviation of all replicates). We calculated integrated daily irradiance as the product of the light intensity ($\mu\text{mol m}^{-2} \text{ s}^{-1}$) and the number of seconds of illumination and convert the units to $\text{mol m}^{-2} \text{ d}^{-1}$.

2.1.2. Cell Physiology

Cells grew exponentially for 5 days and were harvested in the late morning to early afternoon on day 5. This duration was chosen to ensure sufficient material for geochemical and physiological analyses while preventing the cells from encountering nutrient limitation and entering stationary phase. Cell density in each culture vessel was monitored daily using relative fluorescence as a proxy for cell concentration, measured with an AquaFlash fluorometer (Turner Designs, San Jose, CA, USA). 1-mL samples were also collected daily, preserved in paraformaldehyde (1.5%), flash frozen in liquid nitrogen, and stored at -80°C . Preserved samples were subsequently thawed and measured by flow cytometry on a Guava EasyCyte Mini cytometer (Millipore, Darmstadt, Germany) within 6 months. Cell counts from the day of harvest were determined in technical triplicate by microscopy on a hemocytometer. Cellular growth rates (μ , day^{-1}) were calculated from the slope of the relationship between $\ln(\text{cell concentration})$ and time in days after inoculation.

Changes in cell volume between treatments and replicates were constrained using forward scatter estimates from the Guava flow cytometer. Using 1- μm diameter reference beads (Fluoresbrite, YG) to calibrate the flow cytometer response, we compared the forward scatter from aliquots of each culture to the reference

beads and across the range of treatments to examine relative differences. We calculated a response factor by dividing the natural logarithm of the forward scatter of each aliquot to the forward scatter of the reference beads. To convert this relative response factor to a cell volume, we compared all treatments to a “baseline” value. We chose the 400- μatm treatment because it is closest to natural conditions for these cells (mean response factor = 0.75; $n = 3$). We prescribed a mean cell diameter of 5.2 μm for the 400- μatm treatment group—equivalent to a mean cell volume of 73.6 μm^3 —and calculated changes in cell volume relative to this baseline. This prescribed cell diameter is based on eight micrographs of our culture stock of this strain and agrees with measurements of cell diameter of this strain from other batch cultures (Aloisi, 2015; Faucher et al., 2017). We estimated the mean cell volume from each flow cytometry measurement by dividing the response factor (forward scatter of sample relative to standard bead) by the baseline response factor, then multiplying by the prescribed baseline cell volume. We used the standard deviation of the 400- μatm response factor (1 s.d. = 0.07, $n = 3$) as the uncertainty on our estimate and propagated this into a cell diameter uncertainty of $\pm 0.15 \mu\text{m}$. Cell size estimates were corrected for differences in time of sampling between treatments using the approach of Aloisi (2015) (see Equation 5). The cell size at time of sampling and the time-normalized sizes can be found in the Supplementary Material.

2.1.3. Carbonate Chemistry

Carbonate chemistry was monitored using measurements of pH and total alkalinity. The pH of the media in each culture vessel was measured daily using the m-cresol purple method (Dickson et al., 2007) using a Shimadzu UV-1800 spectrophotometer (Kyoto, Japan), calibrated by pH certified reference materials from the Dickson Lab (Scripps Institution of Oceanography, La Jolla, CA, USA). Total alkalinity was assayed by titration at the start and end of the experiment using a closed cell titration with a Metrohm Titrandot autotitrator (Herisau, Switzerland) and calibrated by certified reference materials from the Dickson Lab (Scripps Institution of Oceanography, La Jolla, CA, USA). Alkalinity and pH measurements were made at standard temperature (25°C), and the speciation of the carbonate system was calculated at 18°C using CO2Sys_v2.1 (Lewis & Wallace, 1998). pH is reported on the total scale; we used K_1 and K_2 CO_2 constants of Lueker et al. (2000) with KSO_4 from Dickson and total boron from Uppström (1974).

12-mL samples for dissolved inorganic carbon concentrations and $\delta^{13}\text{C}_{\text{DIC}}$ were taken from each culture vessel at the beginning (t_0) and end (t_f) of the experiments. Samples were sterile filtered through a 0.2- μm polycarbonate filter in a laminar flow hood to remove bacterial contamination from the culture vessels, sealed without headspace in glass vials with septa (model E2852, EA Consumables, Pennsauken, NJ, USA), and shipped to the Stable Isotope Facility at UC Santa Cruz (California, USA) for analysis within 6 months. Each t_0 and t_f sample was analyzed 1 to 8 times. The average precision (average one standard deviation of all replicates) was 100 $\mu\text{mol kg}^{-1}$ for DIC and 0.21 ‰ for $\delta^{13}\text{C}_{\text{DIC}}$. We calculated $\delta^{13}\text{C}_{\text{CO}_2\text{aq}}$ using Equation 2 of Rau et al. (1996). Because cells grew exponentially, the vast majority of the total biomass—and its average carbon isotope ratio—was generated during the last two cell divisions (Figure S7), which is much closer to the t_f measurement than t_0 measurement. We therefore used t_f carbonate chemistry measurements.

2.1.4. Lipid Extraction and Carbon Isotope Measurements

Approximately 150 mL of culture medium from each treatment was gently vacuum-filtered onto pre-combusted glass fiber filters. Free lipids from these filters were extracted via Dionex ASE 350 using a dichloromethane and methanol mixture (9:1 v/v, respectively) at 100°C and 10.3 kPa (1500 psi). The total lipid extract (TLE) was evaporated to dryness under a stream of purified N_2 gas. Alkenone carbon isotope ratios were measured using a Thermo TraceGC coupled to an Isolink device and a Thermo DeltaV mass spectrometer using a J&W DB-1 gas chromatographic column (60 m \times 0.25 mm i.d. \times 0.1 μm phase thickness) and a 10 m guard column. Sample TLEs were injected in toluene into a programmable temperature vaporizing inlet at 90°C, held isothermal for 1.5 min, then heated to 325°C with a splitless time of 5 min, and followed by a cleaning phase with a 50:1 split ratio at 350°C for 5 min. The GC oven temperature started at 90°C, was held isothermal for 1.5 min, ramped 25°C/min to 250°C, then ramped 1°C/min to 313°C, then ramped 10°C/min to 320°C, and held isothermal for 20 min. This method achieved baseline separation of the $\text{C}_{37:2}$ and $\text{C}_{37:3}$ alkenones; here, we only report $\text{C}_{37:2}$ $\delta^{13}\text{C}$ values. An in-line Nafion membrane was used to remove water from the analyte stream. TLE samples were run in duplicate or triplicate. Carbon isotope ratios were translated from the laboratory reference gas scale to the VPDB scale using n -alkane standards of known isotope composition (Mix A5 and Mix B4; produced by A. Schimmelmann, Indiana University), and the uncertainty

in our isotope measurements was calculated using a MATLAB routine based on the method of Polissar and D'Andrea (2014). Sample-specific uncertainties (1 s.d.) are provided in Dataset S1 and are $\leq 0.4\%$.

Because the cultures were contaminated with cotton cheesecloth fibers during sampling, we could not reliably measure bulk particulate carbon or its stable isotope composition. Instead, we estimated cellular $\delta^{13}\text{C}_{\text{POC}}$ using our alkenone carbon isotope data ($\delta^{13}\text{C}_{\text{Mk37:2}}$) and a constant biomass-lipid isotopic offset ($\epsilon_{\text{bio/alk}}$), the same approach as used in sediment studies. We recalculated the weighted-mean $\epsilon_{\text{bio/alk}}$ following the methods of Popp, Kenig, et al. (1998) after Laws (1997) using the published $\delta^{13}\text{C}_{\text{POC}}$ and $\delta^{13}\text{C}_{\text{Mk37:2}}$ data of Popp, Kenig, et al. (1998), Riebesell, Revill, et al. (2000) and Wilkes et al. (2018). The weighting function uses the uncertainties of the $\delta^{13}\text{C}_{\text{POC}}$ and $\delta^{13}\text{C}_{\text{Mk37:2}}$ measurements and gives more weight to values with smaller uncertainties. The standard deviation of this estimated $\epsilon_{\text{bio/alk}}$ is calculated from the inverse square-root of the sum of the inverse of the variances (see Popp, Kenig, et al., 1998, their Table 2). Our new calculations with all available data yielded an $\epsilon_{\text{bio/alk}}$ value of $-4.44\% \pm 0.05\%$, which we applied to our samples to calculate ϵ_p values.

2.2. Culture Compilation and Standardization

2.2.1. Calculating Carbon Demand and Supply

Evaluating the dependence of ϵ_p on cellular carbon demand and diffusive CO_2 supply requires the following parameters: cell size (surface area, volume), particulate organic carbon per cell, cellular growth rate, $[\text{CO}_{2(\text{aq})}]$, the $\delta^{13}\text{C}_{\text{DIC}}$ of the culture media, and the $\delta^{13}\text{C}$ of organic matter ($\delta^{13}\text{C}_{\text{POC}}$) or of alkenones ($\delta^{13}\text{C}_{\text{Mk37:2}}$). We examined carbon isotope fractionation with respect to carbon demand relative to carbon supply using the non-dimensional variable “ τ ” introduced by McClelland et al. (2017) (Equation 2), which is equivalent to the classical carbon demand to diffusive CO_2 supply ratio found in the literature (Burkhardt et al., 1999; Rau et al., 1996). We slightly modified the formulation of τ to explicitly include POC cell⁻¹ and cellular surface area instead of cellular carbon density, because we believe τ defined with these terms better delineates their intrinsic proportionality, though our expressions are mathematically equivalent. We recast τ as:

$$\tau = \frac{\text{POC} \times \mu_i}{\text{SA} \times P_C \times C_e} \quad (2)$$

where POC is the organic carbon content of the cell (mol C), μ_i is the photoperiod-adjusted growth rate of the cell (often termed “instantaneous,” in seconds⁻¹), SA is the surface area over which CO_2 diffuses into the cell (m²), P_C is the permeability of this cell membrane to diffusion of aqueous CO_2 (here we use $2e^{-5} \text{ m s}^{-1}$; see below), C_e is the aqueous CO_2 concentration (mol m⁻³; which requires an estimate or assumption about the density of the culture media, here assumed to be 1023 kg m⁻³).

Photoperiod-adjusted growth rate (μ_i) is calculated by:

$$\mu_i = \frac{\mu \times (L + D)}{L - D \times r} \quad (3)$$

where μ is the specific growth rate (d⁻¹), L and D are the lengths of the light period and the dark period (hours), and r is a coefficient for the effect of respiratory carbon loss in the dark. Here, we take r to be 0.15, following Laws and Bannister (1980) and previous studies (e.g., Riebesell, Revill, et al., 2000; Rost et al., 2002).

2.2.2. Data Compilation

We compiled data from the literature, and in our analysis, only included studies in which all components of τ — CO_2 , POC or cell size, and growth rate—were measured or could be estimated with confidence (Bigdare et al., 1997; McClelland et al., 2017; Popp, Kenig et al., 1998; Popp, Laws, et al., 1998; Riebesell, Revill, et al., 2000; Rost et al., 2002; Wilkes et al., 2018). We did not include the *G. oceanica* data of Rickaby et al. (2010); recent batch culture experiments of *G. oceanica* under similar culture conditions (McClelland et al., 2017) yielded dramatically different $\delta^{13}\text{C}_{\text{POC}}$ results, and McClelland et al. (2017) also excluded the *G.*

oceanica data of Rickaby et al. (2010) in their analysis and interpretation. We also did not include the batch culture experiments of Moolna and Rickaby (2012) because we could not reconcile the reported “end” carbonate system data with the reported $[\text{CO}_{2(\text{aq})}]$: calculating $[\text{CO}_{2(\text{aq})}]$ using the reported DIC and alkalinity returned estimates an order of magnitude higher than the reported $[\text{CO}_{2(\text{aq})}]$. In our multilinear regression models, we did not include the maximum ϵ_p treatment from Bidigare et al. (1997) (24.9‰) because it was achieved at extremely high $[\text{CO}_{2(\text{aq})}]$ (274 μM). It is an important observation and demonstrates that ϵ_p values of ~ 25 ‰ can indeed be achieved, but this CO_2 treatment is unreasonably high for the natural habitat of coccolithophores, is >9 standard deviations away from the mean of the dataset, and exerts exorbitant leverage on the regression coefficients.

2.3. Approach to Constraining τ

Few datasets reported enough information to calculate τ directly. However, this is also the case in sediment studies because input variables, such as POC and cell counts of the alkenone-producing population to calculate POC cell^{-1} are not quantitatively preserved. We approximated components of τ as necessary using well-constrained transfer functions.

2.3.1. Particulate Organic Carbon and Cell Dimensions

There is a robust relationship between algal cell volume and cellular organic carbon content (Montagnes et al., 1993; Popp, Laws, et al., 1998; Verity et al., 1992). These studies used a variety of algal species that covered many orders of magnitude of algal biovolume and found that the relationship between POC cell^{-1} and cell volume followed a power law with the exponent close to one. More targeted work on coccolithophores (Aloisi, 2015), and one study of alkenone-producing algae specifically (McClelland et al., 2017), found a constant organic carbon density of ~ 15 and $18.5 \text{ fmol C } \mu\text{m}^{-3}$, respectively. We use $17.5 \text{ fmol C } \mu\text{m}^{-3} \pm 0.75 \text{ fmol C } \mu\text{m}^{-3}$ to incorporate this range of measured values. Volume and POC are related by:

$$\text{POC} = 17.5 \pm 0.75 \text{ fmol C } \mu\text{m}^{-3} \times V \mu\text{m}^3 \quad (4)$$

where POC is the particulate organic carbon content in femtomole C and V is the cell volume (μm^3). Alkenone-producing coccolithophores are very nearly spherical, and a spherical geometry is commonly employed for these organisms (Bolton et al., 2016; Henderiks & Pagani, 2007; McClelland et al., 2016; Popp, Laws, et al., 1998; Stoll et al., 2019). In treatments where only one of POC cell^{-1} or cell size was reported, we estimated the other parameter using Equation 4. We calculated surface area assuming a spherical cell.

2.3.2. Cell Growth During a Light: Dark Cycle

As emphasized by Aloisi (2015), the time at which samples were collected must be considered when comparing results across experiments and treatments because cell growth and division is synchronized with the light:dark cycle (Müller et al., 2008). Under continuous light, there is no synchronization of cell division, so harvesting the culture at any time draws an unbiased sample from the probability distribution of the different growth phases of the organism. However, cells grown under a discontinuous photoperiod add biomass and increase in size throughout the light period. The time at which the sample is collected can therefore bias the estimate of cell diameter or POC cell^{-1} . To account for differences in sampling time, we used the method outlined in Appendix A1 of Aloisi (2015), which normalizes POC cell^{-1} to a given time in the photoperiod. Here, we normalized to the middle of the photoperiod. POC at a given sample time under a light:dark cycle is calculated by:

$$\text{POC}(t) = \frac{L \times \text{POC}(S_T)}{L + S_T} \times \left(1 + \frac{t}{L} \right) \quad (5)$$

where POC is the particulate organic carbon (pg C), t is the normalization time in hours after the start of the light period, L is the length of the light period in hours, and S_T is the sample collection time in hours after the start of the light period.

2.3.3. Membrane Permeability

To compare the Rau et al. (1996) model to the experimental data in the framework of τ , the cellular carbon demand relative to diffusive CO_2 supply, we require an estimate of the cell membrane permeability to CO_2 diffusion (P_C). This parameter has recently been determined for *Emiliana huxleyi*, with measured values around $1\text{e}^{-4}\text{ m s}^{-1}$ (Blanco-Ameijeiras et al., 2020). However, with this value, the diffusive model solution does not overlap with the data (Figure S9). This suggests that the effective permeability to CO_2 diffusion to RuBisCO (which includes the chloroplast membrane) is lower than the permeability of the cell membrane. We choose a permeability of $2\text{e}^{-5}\text{ m s}^{-1}$ as this visually fits the experimental data on a plot of ε_p versus τ and allows us to show the Rau et al. (1996) model in relation to the data. The exact value is not critical in our overall analysis because it is a constant in τ .

3. Results

3.1. *G. oceanica* Cultures

These batch culture experiments targeted 200, 400, 600, 800, and 1000 $\mu\text{atm pCO}_2$. All treatments were conducted in triplicate (e.g., 200A, 200B, and 200C). We treat each individual cultivation as a unique experiment and conducted all measurements on seawater and particulate matter collected from each vessel. Data are reported in the Supplementary Materials and Dataset S1 and can be found in the DRYAD database (<https://doi.org/10.5061/dryad.bcc2fqzc7>).

3.1.1. Cell Growth

Measured cellular growth rates ranged from 0.78 to 0.99 days^{-1} . Photoperiod-normalized growth rates (using Equation 3) ranged from 1.51 days^{-1} to 1.91 days^{-1} , demonstrating a low-amplitude growth rate response to our experimental range of pCO_2 under the nutrient-replete, constant light, and constant temperature conditions. Maximum growth rates were found at minimum pCO_2 ($201 \pm 3\ \mu\text{atm}$, $0.97 \pm 0.03\ \text{days}^{-1}$; mean \pm one standard deviation of three replicates), while average minimum growth rates occurred in the 800- μatm treatment. In batch cultures of this same strain (RCC1303) at 20°C , Sett et al. (2014) found roughly similar growth rates over a similar pCO_2 range (0.79–1.06 days^{-1} from 280 to 1000 μatm). We note that the 600 ppm treatment yielded more variable growth rates (0.78–0.94 days^{-1} , $\sim 20\%$ variability) than other treatments in our study. Similar relative within-treatment variability was found by McClelland et al. (2017) in biological replicates of *G. oceanica* RCC1211 and RCC1314 CO_2 response experiments. Visualization of cells at the time of harvest confirmed they calcified during these experiments. Final cell concentrations ranged between 1.89×10^4 and $1.24 \times 10^5\ \text{cells mL}^{-1}$, with an average of $6.39 \times 10^4\ \text{cells mL}^{-1}$.

3.1.2. Carbonate Chemistry

The realized pCO_2 was generally slightly lower than the target pCO_2 of each treatment due to biological uptake, which resulted in a pCO_2 range of 168–965 μatm . At 18°C and salinity of 32.53, this results in a $[\text{CO}_{2(\text{aq})}]$ range from 5.8 to 33.4 $\mu\text{mol kg}^{-1}$ (we assume $\pm 10\%$ uncertainty). The mean t_f alkalinity was 2131 $\mu\text{mol kg}^{-1}$ with a standard deviation across all treatments of 47 $\mu\text{mol kg}^{-1}$, and a mean percent changes from t_0 to t_f of 1.75%. The mean pH drift from t_0 to t_f across all treatments was 0.05 units. The carbonate system was therefore relatively chemically stable throughout the majority of the experiments. The largest drift in pH occurred in the 1000C treatment (0.1 units), and the largest drift in alkalinity was found in the 400C treatment (85.5 $\mu\text{mol kg}^{-1}$). The pH and total alkalinity changes are shown in Figure S8, and the initial and final values are reported in Table S2.

We measured the carbon isotope ratio of DIC ($\delta^{13}\text{C}_{\text{DIC}}$) at t_0 and t_f for all experiments. The CO_2 of the culture vessels was set by headspace modification; we continuously pumped air with pre-mixed pCO_2 into the culture vessel directly above the boundary layer of the culture seawater. Because photosynthesis preferentially removes ^{12}C , in a closed system, $\delta^{13}\text{C}_{\text{DIC}}$ values would become more positive as the experiment progresses. However, because our system was open to the atmosphere and continuously purged by ^{13}C -depleted CO_2 , $\delta^{13}\text{C}_{\text{DIC}}$ values became more negative from t_0 to t_f . In some cases (e.g., the 400- μatm experiments), the drift is large, with a maximum of $-9.1\ \%$. However, the vast majority (81%–89%) of the total algal biomass in each treatment is synthesized during the last two cell divisions, with a mean of 62% generated during the final division (Figure S7). Because we do not have a full-time series of carbonate chemistry or $\delta^{13}\text{C}_{\text{DIC}}$, we

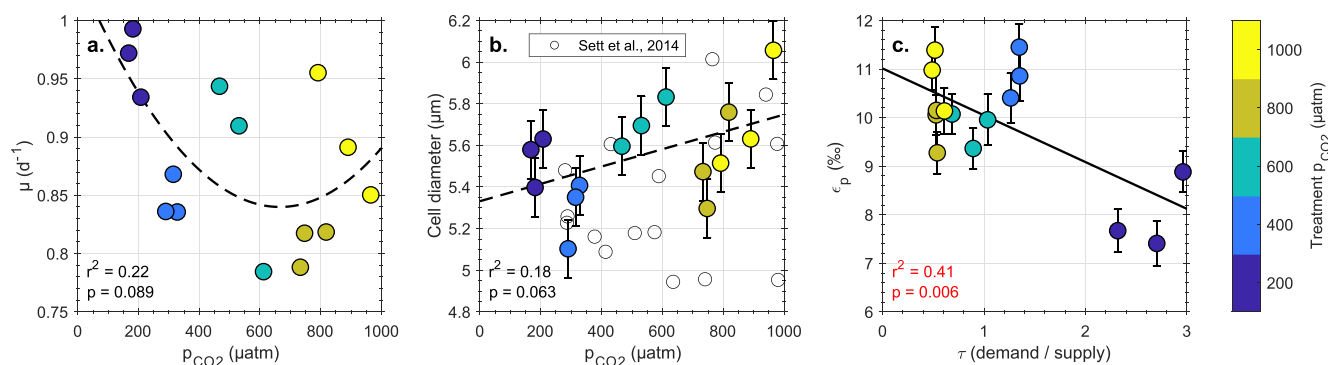


Figure 1. Physiological and geochemical results from *Gephyrocapsa oceanica* (RCC1303) batch cultures (this study). (a) Growth rates with respect to media $p\text{CO}_2$ in batch cultures; dashed black line is a quadratic fit. (b) Estimated cell radius from flow cytometry as a function of $p\text{CO}_2$; dashed line shows linear fit to our culture data. Shown for reference in gray circles are cell diameters estimated using measured POC cell⁻¹ (Equation 4) from Sett et al. (2014) (same strain in batch culture at 20°C). (c) Carbon isotope fractionation (ϵ_p) in our *G. oceanica* cultures determined from alkenone $\delta^{13}\text{C}$ as a function of carbon demand relative to carbon supply. Error bars in (b) and (c) are 1 standard deviation (see methods). Dashed regression lines and black text in panels (a) and (b) indicate statistical significance at the $p < 0.1$ threshold; red text and solid regression line in (c) indicate significance at the $p < 0.05$ level.

use the t_f measurements as the benchmark against which to calculate carbon isotope fractionation (ϵ_p) in our cultures.

3.1.3. Cell Size

Cell diameters estimated from cytometer scattering at the time of sampling ranged from 5.0 to 5.7 μm . When normalized to a common time (the middle of the photoperiod, Equation 5) to account for cell growth and expansion throughout the light period, cell diameters range from 5.1 to 6.1 μm . There was no significant relationship between cell size and $p\text{CO}_2$ across treatments ($r^2 = 0.18$, $p > 0.05$; Figure 1b), although the largest cells were found in the highest $p\text{CO}_2$ treatment (~ 1000 ppm). Our mean cell-size estimates from flow cytometry agree well with POC-estimated cell size from the same strain in the batch cultures of Sett et al. (2014) (Figure 1b) and Faucher et al. (2017) and are therefore representative for nutrient-replete batch cultures of this strain.

3.1.4. Carbon Isotope Fractionation in Organic Matter

Alkenone $\delta^{13}\text{C}$ reflects the source $\delta^{13}\text{C}_{\text{DIC}}$ as well as the effect of CO_2 concentration and physiology on isotope discrimination by RuBisCO. In our cultures, $\delta^{13}\text{C}_{\text{Mk37:2}}$ is highly correlated with $[\text{CO}_{2(\text{aq})}]$ ($r^2 = 0.78$) because the $p\text{CO}_2$ of the culture vessels was established by continuously aerating the headspace with ^{13}C -depleted CO_2 ; this is further evident from the relationship between $\delta^{13}\text{C}_{\text{DIC}}$ and $[\text{CO}_{2(\text{aq})}]$ ($r^2 = 0.83$) (Figure S1). The slope of a linear regression between $[\text{CO}_{2(\text{aq})}]$ and $\delta^{13}\text{C}_{\text{Mk37:2}}$ is $\sim 20\%$ steeper than that of $[\text{CO}_{2(\text{aq})}]$ versus $\delta^{13}\text{C}_{\text{DIC}}$, demonstrating the presence of the CO_2 effect on $\delta^{13}\text{C}_{\text{Mk37:2}}$ in addition to the carbonate system manipulation (Figure S1). This CO_2 effect is clear when isotope fractionation is examined as ϵ_p , the isotope fractionation with respect to $\delta^{13}\text{C}_{\text{CO}_{2(\text{aq})}}$ values (Figure S2). Measured ϵ_p values were between 7.4 and 11.5 ‰, a range comparable to that observed in many batch cultures and in marine sediments of the past ~ 23 Ma (Pagani, 2014; Pagani et al., 2010). As observed in many other datasets, we find an inverse relationship between ϵ_p and $1/[\text{CO}_{2(\text{aq})}]$ (Figure S2). Under these growth conditions, lower growth rates and higher $[\text{CO}_{2(\text{aq})}]$ lead to higher ϵ_p .

3.1.5. Carbon Demand and Diffusive CO_2 Supply

In the conventional framework, carbon demand is set by the photoperiod-normalized growth rate and the carbon content per cell; diffusive supply is calculated as the product of the cellular surface area, the permeability of the cell membrane to CO_2 , and the $[\text{CO}_{2(\text{aq})}]$. Alkenone carbon isotope fractionation and τ are significantly correlated in our dataset, demonstrating a strong effect of physiology and CO_2 supply on alkenone ϵ_p values (Figure 1c). In our culture experiments, τ variations were primarily driven by changing $[\text{CO}_{2(\text{aq})}]$ (a 5.8-fold change) rather than growth rate, and ranged from approximately 0.5 to 3. The strongest correlation between ϵ_p and the components of τ was found with $1/[\text{CO}_{2(\text{aq})}]$ (Figure S2). Estimated cell radius varied by less than 20% across treatments, and photoperiod-normalized growth rate changed by a maximum of $\sim 25\%$.

Our results support the foundational observations that carbon isotope fractionation carries a signature of the ambient $[\text{CO}_{2(\text{aq})}]$. However, our experiments covered a small ϵ_p range and did not reach low τ values where carbon demand is very low relative to supply, so we are unable to determine the continuity of the ϵ_p response to τ from our experiments alone.

3.2. Culture Synthesis

We synthesized existing culture data of alkenone-producing coccolithophores that reported ϵ_p values and sufficient physiological information and metadata to estimate τ in each sample. These additional data include *E. huxleyi* strains BT6 (Bidigare et al., 1997; Popp, Kenig, et al., 1998; Popp, Laws, et al., 1998), PML B92/11 (Bidigare et al., 1997; Popp, Kenig, et al., 1998; Popp, Laws, et al., 1998; Riebesell, Revill, et al., 2000; Rost et al., 2002), RCC1216, and RCC1256 (McClelland et al., 2017), and *G. oceanica* strains RCC1211, and RCC1314 (McClelland et al., 2017). While there may be differences at the strain level, including data from all strains in our analysis is most applicable to sediment studies, as one cannot distinguish alkenones at the strain level in the sedimentary record. Our synthesis, accounting for differences in sampling times, permits a robust evaluation of the carbon isotope response of alkenone-producing algae to changes in CO_2 supply and cellular carbon demand. In this dataset, ϵ_p values range from ~ 7 to ~ 23 ‰, consistent with alkenone ϵ_p records from the Cenozoic (Pagani, 2014). Calculated τ values span ~ 2 orders of magnitude (~ 0.1 to ~ 6 units; absolute values depend on the choice of membrane permeability because the membrane permeability is a multiplier on the denominator of τ).

Combining our *G. oceanica* data with published Noelaerhabdaceae ϵ_p data, we observe a highly scattered inverse relationship between ϵ_p and τ . This indicates that diffusive CO_2 supply—or CCM activity that responds to the ambient CO_2 concentration like diffusive supply—is one aspect controlling carbon isotope fractionation. In contrast, we observe a strong effect of irradiance (photoperiod and light intensity) on ϵ_p values. At low values of τ (< 1), the compiled culture data span a wide range of photoperiod and irradiance values, and we observe a large range in ϵ_p values: both the maximum and minimum ϵ_p and irradiance values occur at $\tau < 0.2$. Across these cultures, where light conditions are different, the variability in ϵ_p values is more closely related to irradiance than τ (Figure 2b). The influence of irradiance on ϵ_p is not apparent at high τ values because the range of irradiance values in this subset of experiments is comparatively small (~ 5 – 11 mol photons $\text{m}^{-2} \text{d}^{-1}$).

4. Discussion

Our analysis of existing and new ϵ_p and τ determinations from cultures of alkenone-producing algae demonstrates a number of relationships that will be important to address in the paleoenvironmental interpretation of alkenone ϵ_p values:

- (i) ϵ_p as a function of τ is poorly predicted by the linear Rau et al. (1996) model used in the alkenone- CO_2 proxy,
- (ii) while there is a CO_2 effect on ϵ_p , variance in ϵ_p across cultures is better explained by irradiance than τ ,
- (iii) the values of ϵ_p in many cultures exceed the value of in vitro $\epsilon_{\text{RuBisCO}}$ measured in the alkenone-producing *E. huxleyi* (Boller et al., 2011).

Here, we present an empirical analysis of the relationship between ϵ_p and τ , where we consider the ability of the diffusive model—the traditional framework for the alkenone paleobarometer—to explain the measured ϵ_p data. We then evaluate the influence of irradiance on ϵ_p through multiple linear regression analysis, demonstrating a significant role of both light intensity and photoperiod in determining photosynthetic carbon isotope fractionation. Finally, we conclude with a discussion of future directions for alkenone carbon isotope ratios as a proxy of past environmental conditions.

4.1. Sensitivity of ϵ_p to Carbon Demand and Supply (τ)

The alkenone paleobarometer invokes a linear relationship between carbon isotope fractionation (ϵ_p) and carbon demand relative to carbon supply (τ) (Bidigare et al., 1997; Pagani et al., 2000; Popp, Laws, et al., 1998; Rau et al., 1996). Overall, the highest ϵ_p values only occur at low τ values, and high τ is associated with low ϵ_p

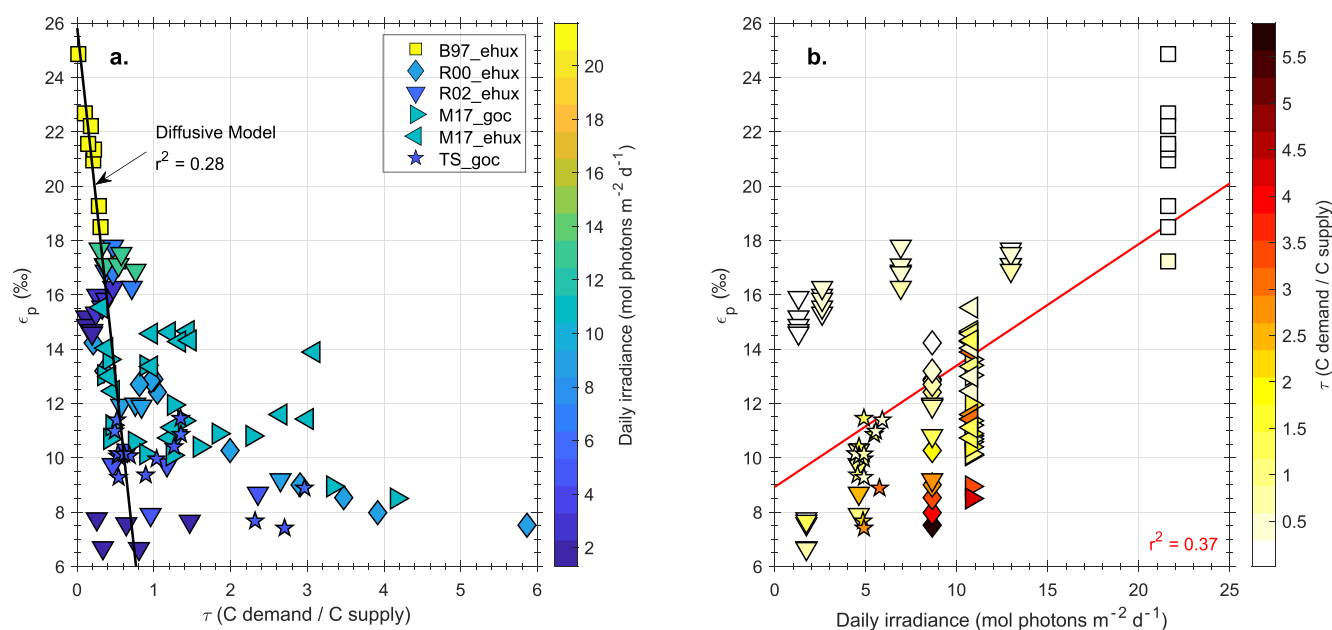


Figure 2. Carbon isotope fractionation in organic matter (ϵ_p) from *G. oceanica* cultures (this study) and published data from other alkenone-producing algae. (a) ϵ_p plotted against carbon fixation relative to diffusive CO_2 supply (τ), colored by total daily irradiance. Black line is the solution using the Rau et al. (1996) diffusive model (Equation 1). (b) ϵ_p as a function of total daily irradiance, colored by τ . Red line is an ordinary linear regression. Symbols are the same in both panels and indicate the publication and species, where the abbreviation is the first initial of the first author's last name, the publication year, and the species studied (ehux = *Emiliana huxleyi*; goc = *Gephyrocapsa oceanica*). “TS” is “This Study.” Error bars omitted for clarity. The diffusive model poorly predicts ϵ_p as a function of τ ; more variance in ϵ_p can be explained by irradiance than the diffusive model.

values. This relationship is an important feature of the dataset: it suggests that organic carbon isotope fractionation by alkenone-producing algae is indeed recording information about the cellular carbon budget, including ambient $[CO_{2(aq)}]$. This general finding echoes the observations of many individual studies and the *G. oceanica* data we present here, in which increasing τ leads to lower ϵ_p values. There is, therefore, utility in algal paleobarometry if other physiological and environmental factors can be constrained. However, the diffusive model does not accurately predict isotope fractionation: as τ increases, the modeled rate of diffusion of $CO_{2(aq)}$ through the boundary layer is insufficient to support cell growth. This implies that the model is not properly parameterized, or CCMs are enhancing carbon supply beyond what is possible by simple diffusion, which is suggested to occur at low CO_2 concentrations (Bach et al., 2013; Isensee et al., 2014). Furthermore, applications of the alkenone paleobarometer that attempt to account for changes in cell size or growth rate (e.g., Pagani et al., 2000; Henderiks and Pagani, 2007) following the scaling factors of Popp, Laws, et al. (1998) would only be valid if the ϵ_p response was accurately and universally described by the linear diffusive model.

While the data in aggregate show ϵ_p values decrease as τ increases, there are differences between ϵ_p , τ , and irradiance across studies that underpin the observed combined response. To evaluate how the range of experimental conditions in each study affects ϵ_p , we conduct a meta-analysis to isolate the slope of ϵ_p versus τ in each treatment (Figure 3). We define a “treatment” as a unique combination of lab, algal strain, and light conditions. From five studies with sufficient data to calculate the statistics on this relationship, there are 16 unique treatments, which subject a total of four strains of *E. huxleyi* and three strains of *G. oceanica* to various CO_2 conditions. We find that the slope of ϵ_p versus τ decreases as the mean τ value in the treatment increases, and that all slopes are either negative (decreasing ϵ_p with increasing τ) or indistinguishable from 0 at the 90% confidence level (Figure 3). Therefore, the τ range of the treatment is important in determining the amplitude of the ϵ_p response and further highlights that the ϵ_p data are not described by a universal linear function of τ . As shown in Figure 2, more of the variance in ϵ_p is explained by the total daily irradiance in the cultures than by τ . The meta-analysis shows that irradiance is also an important determinant of the magnitude of the slope, even at very similar τ values: between τ of 0 and 1, the slope of ϵ_p versus τ

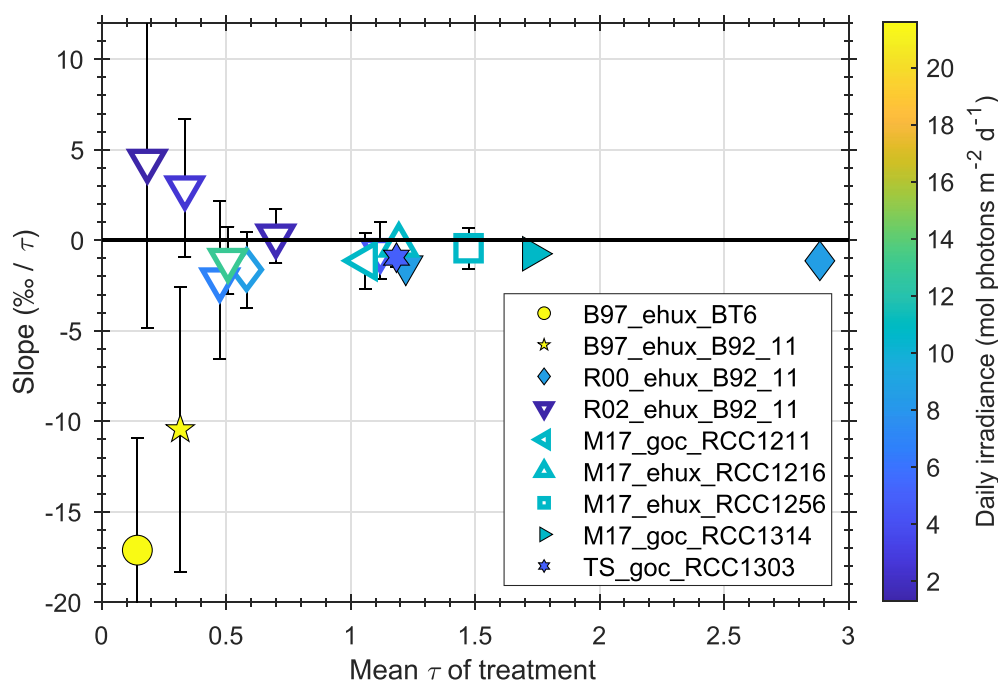


Figure 3. Meta-analysis of individual experimental treatments in cultures of alkenone-producing algae. Slope of the ϵ_p - τ relationship in each treatment is plotted as a function of the mean τ in each treatment. Error bars are 90% confidence intervals on the slope; symbols are colored by total daily irradiance. Filled symbols have ϵ_p versus τ slopes that are different from 0 at the 90% confidence level. Legend abbreviations are similar to Figure 2, with the first initial of the first author's last name, year of publication, species studied, and algal strain. There are more symbols than legend entries because one study (Rost et al., 2002) has multiple light conditions for the same strain. Statistics of the meta-analysis are reported in Table S3.

encompasses the full slope range in the dataset, with more negative slopes at higher irradiance conditions, and lower slopes at lower irradiance. We caution that the combination of high τ (>1) and high irradiance ($>15 \text{ mol photons m}^{-2} \text{ d}^{-1}$) does not exist in these data, and thus we cannot confirm that the observed relationship occurs for all combinations of τ and light. However, there is a clear dependence of ϵ_p on irradiance that is not accounted for in the diffusive model and the conventional alkenone paleobarometer (Rost et al., 2002).

Some authors have argued that deviation from a linear ϵ_p versus τ relationship is indicative of non-diffusive CO_2 supply (Keller & Morel, 1999; Laws et al., 1997; 2002; Stoll et al., 2019). The apparent asymptote in carbon isotope fractionation as τ increases suggests that at high τ , the photosynthetic apparatus reaches a CO_2 threshold below which carbon fixation does not proceed because O_2 outcompetes CO_2 at the active site of RuBisCO (Raven, 1997). Approaching this threshold where CO_2 becomes less available, algae rely more heavily on import and/or transport of HCO_3^- across intracellular membranes to meet their carbon fixation requirement (Anning et al., 1996; Bach et al., 2013; Holtz et al., 2015; 2017; McClelland et al., 2017). HCO_3^- movement follows facilitated diffusion or active transport pathways because it is a charged species. It is then converted to CO_2 —likely by the enzyme carbonic anhydrase (CA) (Mackinder et al., 2011; Quiroga & González, 1993) or through acid-base equilibrium set by internal pH gradients (Falkowski & Raven, 2007; Holtz et al., 2015)—and used for carbon fixation. This type of CCM has been termed the “chloroplast pump model” (Hopkinson, 2014). Greater HCO_3^- uptake at higher τ values would raise the chloroplast CO_2 concentration above what is expected or possible from CO_2 diffusion alone (Bach et al., 2013; Bolton & Stoll, 2013; Hopkinson et al., 2011; Isensee et al., 2014). At thermodynamic equilibrium in seawater, CO_2 $\delta^{13}\text{C}$ values are approximately 10 ‰ lower than HCO_3^- $\delta^{13}\text{C}$ values. Dehydration of HCO_3^- by CA imparts a -10.1 ‰ isotope effect, generating CO_2 that is isotopically similar to ambient equilibrium CO_2 (Riebesell & Wolf-Gladrow, 1995). This type of CCM is therefore isotopically undetectable and it appears as an artificial enhancement of CO_2 concentrations (Zeebe & Wolf-Gladrow, 2001). Other CCMs may indeed be active and responsible for some of the ϵ_p variance we see, but we do not have measurements to directly test for them.

Another explanation for the deviation from the diffusive model invokes changes in the cell membrane permeability to CO₂. Measurements of *E. huxleyi* cell membrane permeability to CO₂ found no plasticity in incubations at 14°C with 150 and 1000 ppm CO₂, and nearly a doubling of permeability from 150 to 1000 ppm CO₂ at 22°C (Blanco-Ameijeiras et al., 2020). However, Stoll et al. (2019) demonstrated coccolithophores would have to plastically modify membrane permeability by over two orders of magnitude to explain the ϵ_p data using the diffusive model, which suggests variable membrane permeability is insufficient.

4.2. Kinetic Fractionation by RuBisCO and Implications for the Diffusive Model

The premise of the diffusive model is that the kinetic fractionation by RuBisCO ($\epsilon_{\text{RuBisCO}}$) sets the maximum possible ϵ_p , fractionation associated with CO₂ diffusion sets the minimum possible ϵ_p , and carbon demand relative to CO₂ supply defines the slope of the line between these two values. The maximum measured ϵ_p values approach 25 ‰, yet in vitro measurements of $\epsilon_{\text{RuBisCO}}$ isolated from *E. huxleyi* yielded ~11 ‰ (95% CI: 9.8–12.6 ‰) (Boller et al., 2011). In vitro measurements of RuBisCO isolated from marine diatom *S. costatum*, which also expresses the form ID RuBisCO found in *E. huxleyi*, yielded a value of 18.5 ‰ (95% CI: 17.0–19.9 ‰) (Boller et al., 2015). Alkenone ϵ_p values exceeding $\epsilon_{\text{RuBisCO}}$ ($\epsilon_p > 11\text{‰}$) are common in cultures, the modern ocean, and Cenozoic marine sediments. The diffusive model cannot explain these observations. It is possible that the in vitro measurements are not representative of in vivo RuBisCO fractionation in *E. huxleyi* and *S. costatum*. However, there is no reason to assume this is the case, and the $\epsilon_{\text{RuBisCO}}$ measurements suggest that additional fractionation steps occur before fixation by RuBisCO to modify the carbon isotope composition of the internal DIC pool.

The observed variation in form ID RuBisCO carbon isotope fractionation is a fundamental hurdle to a mechanistic understanding of algal $\delta^{13}\text{C}$ values. Given that model alkenone-producer *E. huxleyi* and marine diatom *S. costatum* both possess form ID RuBisCO, why are their measured $\epsilon_{\text{RuBisCO}}$ values so different? Further, if there is such diversity in form ID $\epsilon_{\text{RuBisCO}}$, could other alkenone-producing coccolithophores (e.g., *G. oceanica* and its ancestors) have dramatically different $\epsilon_{\text{RuBisCO}}$ values than that measured in *E. huxleyi* by Boller et al. (2011)? It is plausible that carbon isotope fractionation is related to the genetic diversity of the RuBisCO amino acid sequences that encode the catalytic activity of this enzyme. The active site of carboxylation is found at the union of two large subunits of RuBisCO (Andersson, 2008). Phylogenies for the *rbcl* genes encoding the large subunit of RuBisCO place haptophytes and diatoms as distinct groups (Young et al., 2012), perhaps consistent with the ~7 ‰ difference in $\epsilon_{\text{RuBisCO}}$ measurements of these groups. However, *G. oceanica* and *E. huxleyi* are statistically indistinguishable in their *rbcl* and *rbcs* (small subunit gene) phylogenies (Young, 2011), suggesting features of RuBisCO activity, including carbon isotope fractionation, may be conserved. Our observation of a relatively consistent ϵ_p signal across strains with respect to changing τ and irradiance suggests that non-RuBisCO fractionation processes are conserved as well. Either $\epsilon_{\text{RuBisCO}}$ varies with τ systematically across the strains that we have examined here, or ϵ_p is indeed recording changes in τ and light for mechanistic reasons that are still being uncovered. In lieu of a robust mechanistic explanation of carbon isotope fractionation, empirical relationships provide a framework for extracting paleoenvironmental information from alkenone carbon isotope fractionation.

4.3. What Explains Variations in ϵ_p ?

Wilkes and Pearson (2019) proposed that a photocatalytic CCM, which is more active at high light intensity and low nutrient conditions, is responsible for the large isotope fractionation in chemostat experiments. High irradiance and low nutrient conditions must therefore result in more ¹³C-depleted DIC in the vicinity of RuBisCO. Their model, which includes a biochemical fractionation step during hydroxylation of CO₂ to HCO₃⁻ during transit across the thylakoid membrane under high photon flux, was able to explain a large proportion of the observed culture ϵ_p data across several algal groups. In contrast to a mechanistic approach, empirical models can help identify which parameters can explain the observed variance in ϵ_p values. Below we take an empirical approach to predict ϵ_p values and consider the roles of carbon demand and carbon supply as well as irradiance.

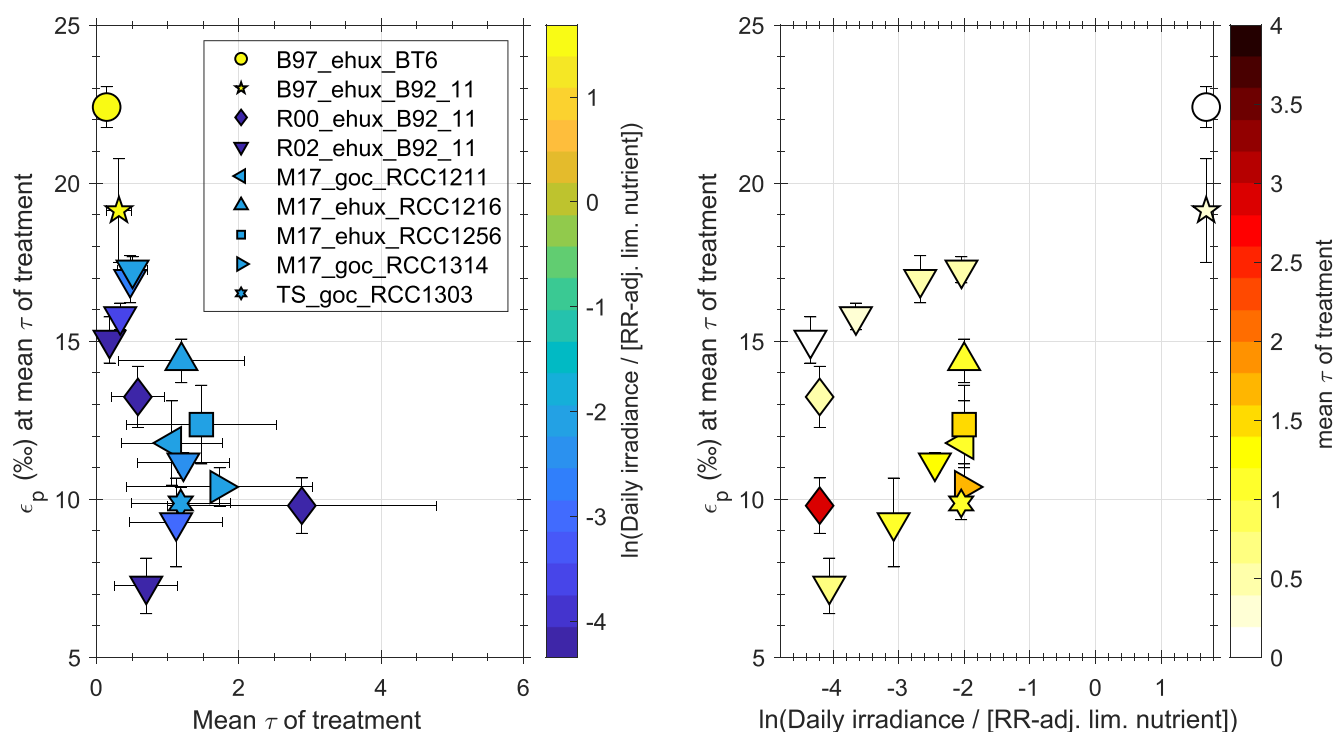


Figure 4. Calculated carbon isotope fractionation (ϵ_p) at the mean τ of each treatment with respect to (a) the mean τ of each treatment, (b) ratio of daily irradiance to the Redfield ratio-adjusted limiting nutrient concentration in the culture media. Error bars on ϵ_p are 95% confidence intervals on the predicted ϵ_p value at the mean τ value based on the linear fit from the meta-analysis. Horizontal error bars in (a) show the maximum and minimum τ values in the treatment. Legend abbreviations follow Figure 3. Symbols in (a) are colored by the natural log of the ratio of light to Redfield ratio-adjusted limiting nutrient concentration; symbols in (b) are colored by the mean τ of the treatment.

The diffusive model, in which ϵ_p is a linear function of τ with an intercept of $\sim 25\%$, can only explain $\sim 28\%$ of the variance in ϵ_p (Figure 2a; black line). With 72% of the variance unexplained, other factors must also play a role in determining carbon isotope fractionation. Fundamental parameters for algal growth, including nutrient concentrations, light intensity, and temperature, are likely candidates. The highest ϵ_p values ($>20\%$) were achieved under nutrient-limited, continuous, and high-intensity light experiments (Bidigare et al., 1997; Popp, Laws, et al., 1998; Wilkes et al., 2018). The next highest ϵ_p values ($\sim 18\%$) were achieved in the (nutrient-replete) batch incubations of Rost et al. (2002), which were also grown under continuous light at relatively high light intensity ($150 \mu\text{mol m}^{-2} \text{s}^{-1}$). Most batch cultures with a light-dark cycle yield ϵ_p values between 8 and 14% (Riebesell et al., 2000; Rost et al., 2002; McClelland et al., 2017; this study). Across the compiled culture dataset, we see a significant relationship between ϵ_p values and the integrated daily irradiance ($\mu\text{mol photons m}^{-2} \text{d}^{-1}$), where higher ϵ_p values occur at higher total daily irradiance (Figure 2b). The data, particularly the low-light experiments of Rost et al. (2002) (dark blue inverted triangles, Figure 2a), also demonstrate that high CO_2 supply relative to demand (low τ) is necessary for achieving high ϵ_p values, but it is not sufficient on its own.

We explore the role of light and nutrients by examining the relationship between ϵ_p at the mean τ of each treatment and the ratio of daily irradiance to the Redfield ratio-adjusted minimum nutrient concentration in the growth medium (Figure 4). We find that both τ and light/nutrients affect ϵ_p . At a constant τ , lower ϵ_p values correspond to low light and high nutrient concentrations (Figure 4a), while at a constant light to nutrient ratio, lower τ values correspond to higher ϵ_p values (Figure 4b). This analysis emphasizes that high light/low nutrient conditions appear necessary to produce the highest ϵ_p values. Some studies have suggested a greater reliance on bicarbonate at lower irradiance and shorter daylength (Rost et al., 2006), raising a question of where the energy required for such photocatalytic CCM activity is derived. Possibly these algae are sacrificing inorganic carbon production for organic carbon production at low irradiance. Analysis by Krumhardt et al. (2017) shows that PIC/POC in *Emiliania huxleyi* generally increases as irradiance increases. It is therefore possible that at lower light and shorter daylengths, energy used for calcification

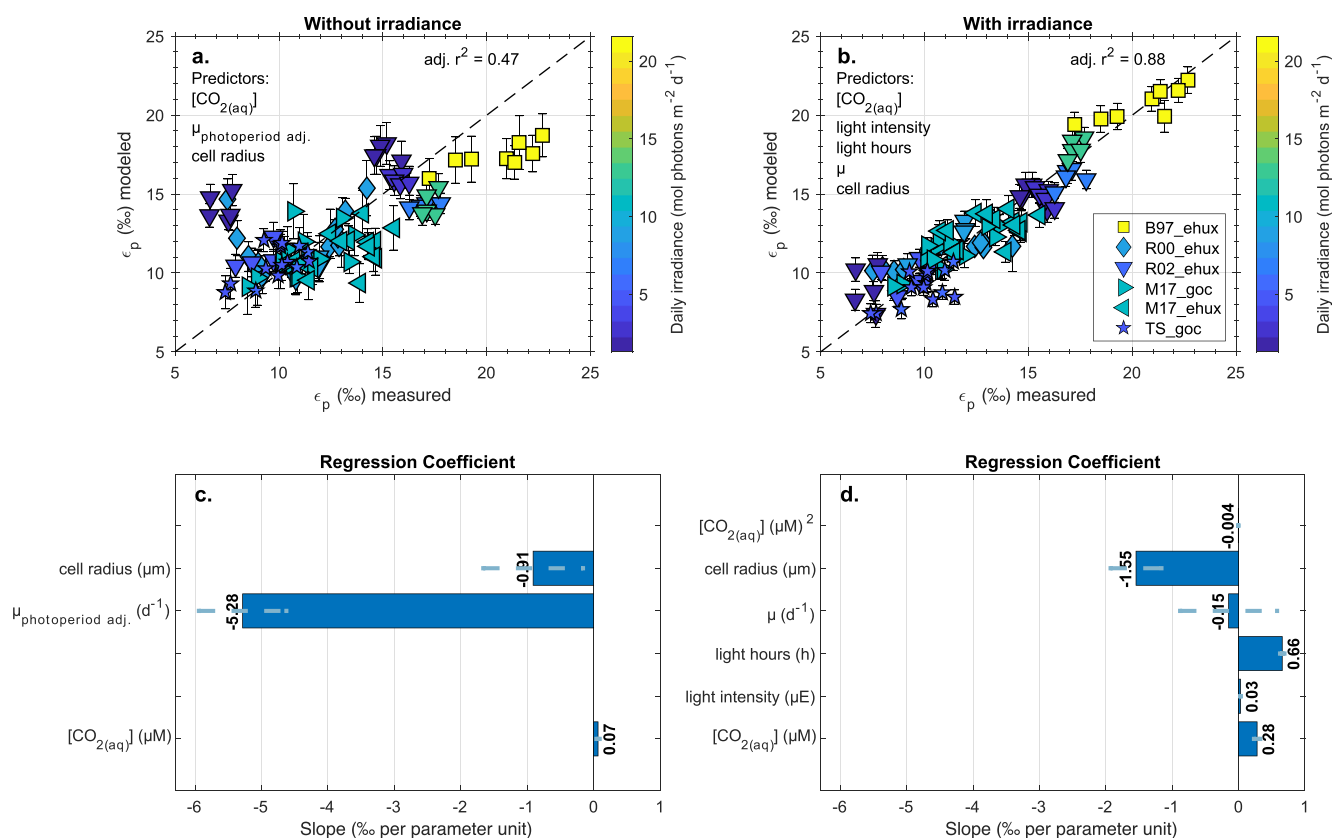


Figure 5. Multiple linear regression models to predict ϵ_p values in cultures of alkenone-producing algae. Error bars show the 95% confidence intervals on modeled ϵ_p values. Samples are colored by integrated daily irradiance. (a) Predictor variables include only the components of τ . (b) Predictor variables add light intensity ($\mu\text{mol photons m}^{-2} \text{s}^{-1}$) and light duration (hours), and use growth rate (μ) instead of photoperiod-adjusted growth rate ($\mu_{\text{photoperiod adj.}}$ or μ_i) because photoperiod is an independent parameter in this model. (c) and (d) show the magnitude and value of the coefficients for each predictor variable in the linear regressions for (a) and (b) respectively. Dashed lines indicate 66% confidence intervals on the estimate of the coefficient value.

is redirected to support organic matter production. Bolton and Stoll (2013) showed that HCO_3^- was likely reallocated away from calcification and to photosynthesis as CO_2 declined. This process could be operating at lower irradiance as well. Furthermore, this phenomenon could be associated with enhanced production of lipids (which are ^{13}C -depleted relative to biomass) under high light intensities, though a modeling study required likely unreasonably large lipid fractionation factors and over-parameterization to produce large irradiance-driven variations in ϵ_p (Holtz et al., 2017).

Although we do not have direct experimental evidence for the mechanism of an irradiance effect on carbon isotope fractionation, we can probe the influence of light in addition to carbon demand and supply through multivariate linear regressions (Stoll et al., 2019). First, we develop a linear regression model to predict ϵ_p values from the components of τ : photoperiod-normalized growth rate (μ_i), cell radius, and $[CO_{2(aq)}]$. With these variables, we are able to model $\sim 47\%$ of the variance in the ϵ_p data (Figure 5a). This model is markedly improved if we include the light parameters. We can explain $\sim 88\%$ of the variance in ϵ_p if we instead model ϵ_p as a function of growth rate (μ), cell radius, $[CO_{2(aq)}]$ (and a quadratic term), the light intensity, and light hours (Figure 5b). We allow for a quadratic term in $[CO_{2(aq)}]$ because it improves the quality of the fit and the sensitivity of ϵ_p to $[CO_{2(aq)}]$. A third model that uses the integrated daily irradiance instead of light hours and light intensity also performs better than the τ model ($r^2 = 0.65$; Figure S6). We elect to use light hours and cellular growth rate (μ) rather than photoperiod-normalized growth rate (μ_i) because μ_i is a function of photoperiod and requires an assumption about the magnitude of respiratory carbon loss in the dark (see Equation 3). Consistent with previous work, the linear regression models also identify a strong sensitivity of ϵ_p to cell radius. The irradiance model (Figures 5b and 5d) shows ϵ_p values decline by 1.55 ‰ for each 1- μm increase in cell radius. These regression models indicate that light intensity and duration as well as

cell size are essential parameters for predicting carbon isotope fractionation in alkenone-producing algae (independent of their effects on growth rate) and must be considered in natural samples.

4.4. Next Steps for the Alkenone ϵ_p Paleobarometer

It would be advantageous to continue to use alkenone carbon isotope fractionation in ancient sediments to estimate past atmospheric CO_2 concentrations. The limit of maximum ϵ_p at 25 ‰ was previously explained by CO_2 supply in such excess of CO_2 demand that carbon fixation was the rate-limiting step in CO_2 consumption, leading to a full expression of the kinetic fractionation by RuBisCO. However, if $\epsilon_{\text{RuBisCO}}$ in alkenone-producing algae is ~ 11 ‰ (Boller et al., 2011), more complex mechanisms must be at play, such as the photocatalytic CCM proposed by Wilkes and Pearson (2019). Measurements to identify these mechanisms should be a target of future culture studies and field campaigns.

At present, the data suggest that the diffusive model is not accurately predicting the response of ϵ_p to CO_2 change. As a consequence, it does not describe the quantitative scaling between growth rate, cell size, and ϵ_p . Empirical calibrations, like the ones presented in Figures 2 and 5, are useful, but paleoreconstructions using these calibrations are only as strong as their calibration treatment matrix. There is a clear distinction in the ϵ_p and τ space that is occupied by different culture conditions: chemostats tend to produce the highest ϵ_p and lowest τ values, while batch cultures generally yield lower ϵ_p and higher τ values. Conditions like those in the chemostat cultures in our analysis (high-intensity, 24-h light) are rarely achieved in the ocean—especially not in the subtropical regions that are oceanographically suited for reconstructing atmospheric CO_2 . With growth rates between ~ 0.1 and 1 day^{-1} and modern $\text{CO}_{2(\text{aq})}$ concentrations and cell sizes, τ would range between ~ 0 and 2 units, though τ values may have been higher in times of lower CO_2 (glacial periods), or when Noelaerhabdaceae cell sizes were larger, as is the case in much of the Cenozoic (Henderiks & Pagani, 2007; 2008; Herrmann & Thierstein, 2012). In this plausible “Cenozoic-equivalent” τ range, we observe a stronger dependence of ϵ_p on irradiance than in the full dataset and an even weaker dependence on τ (Figure S10), suggesting irradiance may be significant in marine settings as well. For these reasons, we recommend caution in the use of the diffusive model and its modifications for CO_2 reconstructions.

The influence of irradiance presents an additional hurdle because there is no robust paleoproxy for irradiance at the depth of alkenone production. Modern surveys demonstrate that alkenone production generally occurs within the upper water column (0–100 m), but the depth of maximum alkenone export production is spatially variable and does not strictly follow in-situ irradiance profiles (Ko et al., 2018; Lee et al., 2014; Lee & Schneider, 2005; Popp et al., 2006; Wolhowe et al., 2014). Because irradiance decreases exponentially with depth, it is plausible that the average irradiance conditions contributing to alkenone production and the sedimentary ϵ_p signal have changed through time. Sediment samples integrate hundreds to thousands of years of alkenone production, and may average annual and seasonal irradiance variations in a way that is not straightforward. An alkenone-based proxy could provide a contemporaneous constraint on the irradiance signature in alkenone $\delta^{13}\text{C}$ records. Some culture experiments suggest the hydrogen isotope ratios ($\delta^2\text{H}$) of alkenones record a signature of irradiance conditions during growth, though salinity, growth rate, and species also influence alkenone $\delta^2\text{H}$ values (van der Meer et al., 2015; Schouten et al., 2006; Weiss et al., 2019). In the natural environment, Wolhowe et al. (2015) found more negative alkenone $\delta^2\text{H}$ values deeper in the water column, consistent with lower irradiance. While promising, more work is necessary to disentangle the multiple controls of alkenone $\delta^2\text{H}$.

In order to apply these empirical relationships to sediments with confidence, future work should focus on identifying whether the factors investigated here (carbon economics and light energy) are indeed the primary determinants of carbon isotope fractionation in algae in the modern ocean. There is an abundance of alkenone carbon isotope data from marine particulates and core-top sediments, but our analysis shows that previous validation studies (e.g., Pagani et al., 2002) have not yet rigorously tested the fundamental principles of carbon isotope fractionation in these algae. That analysis is beyond the scope of this study, but will be the focus of future work.

5. Conclusions

The alkenone paleobarometer is one of a handful of methods for estimating past atmospheric CO₂ concentrations. The quantitative framework of the proxy assumes (1) that alkenone-producing algae acquire carbon solely through diffusion, (2) the extent of carbon isotope fractionation ranges between the kinetic fractionation by the carboxylating enzyme RuBisCO and the fractionation of aqueous CO₂ diffusion, and (3) isotope fractionation is linearly proportional to CO₂ availability. We use culture experiments of alkenone-producing *G. oceanica* in conjunction with a rigorous compilation of existing culture data to test these fundamental underpinnings of the alkenone paleobarometer. Within tightly controlled experimental conditions (species, strain, light treatment), we find a dependence of ϵ_p on carbon demand relative to carbon supply, indicating that CO₂ information is indeed recorded in the carbon isotope fractionation of these algae. However, the relationship differs with irradiance and carbon demand relative to supply, indicating additional processes are affecting carbon isotope fractionation. We show that including irradiance can explain almost half (~40%) of the variance in the ϵ_p data. The strong covariance between light and ϵ_p suggests the occurrence of irradiance-dependent isotope fractionation beyond the effect of light on growth rate. Applications of the alkenone paleobarometer must take the effects of irradiance into account. We report empirical relationships between ϵ_p and irradiance, cell size, CO₂, and growth rate. With appropriate validation it may be possible to reconstruct past changes in CO₂ using these relationships.

Conflict of Interest

The authors declare no conflicts of interest relevant to this study.

Data Availability Statement

The data supporting this study are available in the DRYAD database (<https://doi.org/10.5061/dryad.bcc2fqzc7>).

Acknowledgments

This work was supported by the Center for Climate and Life at Columbia University, as well as the Lamont Climate Center and the G. Unger Vetlesen Foundation. SRP was supported by a U.S. National Science Foundation graduate research fellowship (grant no. DGE16-44869). Additional support was provided by the National Science Foundation Biological Oceanography Program (Grant no. OCE1314336, STD), with partial support also provided by WSL Pure in partnership with Columbia University's Center for Climate and Life, the Paul M. Angell Family Foundation, Columbia Earth Institute Research Assistantship (OMW), and The Columbia University Bridge to PhD Program in the Natural Sciences Research Assistantship (MDHL). We thank Hugh Ducklow and Naomi Shelton for the use of and training on the autotitrator and Andrew Juhl for contributions to the original experimental design and construction of a CO₂ flowmeter manifold. We thank Heather Stoll, Peter deMenocal, Bärbel Hönlisch, Andrew Juhl, and Ann Pearson for constructive comments on the manuscript, and Wei Huang for laboratory assistance. The authors also thank three anonymous reviewers whose thorough comments improved the quality and presentation of this manuscript.

References

- Aloisi, G. (2015). Covariation of metabolic rates and cell size in coccolithophores. *Biogeosciences*, *12*(15), 4665–4692. <https://doi.org/10.5194/bg-12-4665-2015>
- Andersson, I. (2008). Catalysis and regulation in Rubisco. *Journal of Experimental Botany*, *59*(7), 1555–1568. <https://doi.org/10.1093/jxb/ern091>
- Anning, T., Nimer, N., Merrett, M. J., & Brownlee, C. (1996). Costs and benefits of calcification in coccolithophorids. *Journal of Marine Systems*, *9*(1–2), 45–56. [https://doi.org/10.1016/0924-7963\(96\)00015-2](https://doi.org/10.1016/0924-7963(96)00015-2)
- Bach, L. T., Mackinder, L. C. M., Schulz, K. G., Wheeler, G., Schroeder, D. C., Brownlee, C., & Riebesell, U. (2013). Dissecting the impact of CO₂ and pH on the mechanisms of photosynthesis and calcification in the coccolithophore *Emiliana huxleyi*. *New Phytologist*, *199*(1), 121–134. <https://doi.org/10.1111/nph.12225>
- Badger, M. P. S. (2021). Alkenone isotopes show evidence of active carbon concentrating mechanisms in coccolithophores as aqueous carbon dioxide concentrations fall below 7 μmolL⁻¹. *Biogeosciences*, *18*(3), 1149–1160. <https://doi.org/10.5194/bg-18-1149-2021>
- Badger, M. P. S., Chalk, T. B., Foster, G. L., Bown, P. R., Gibbs, S. J., Sexton, P. F., et al. (2019). Insensitivity of alkenone carbon isotopes to atmospheric CO₂ at low to moderate CO₂ levels. *Climate of the Past*, *15*(2), 539–554. <https://doi.org/10.5194/cp-15-539-2019>
- Badger, M. R., Andrews, T. J., Whitney, S. M. M., Ludwig, M., Yellowlees, D. C., Leggat, W., & Price, G. D. (1998). The diversity and coevolution of Rubisco, plastids, pyrenoids, and chloroplast-based CO₂-concentrating mechanisms in algae. *Canadian Journal of Botany*, *76*(6), 1052–1071. <https://doi.org/10.1139/b98-074>
- Bae, S. W., Lee, K. E., & Kim, K. (2015). Use of carbon isotopic composition of alkenone as a CO₂ proxy in the East Sea/Japan Sea. *Continental Shelf Research*, *107*, 24–32. <https://doi.org/10.1016/j.csr.2015.07.010>
- Balch, W. M., Holligan, P. M., & Kilpatrick, K. A. (1992). Calcification, photosynthesis and growth of the bloom-forming coccolithophore, *Emiliana huxleyi*. *Continental Shelf Research*, *12*(12), 1353–1374. [https://doi.org/10.1016/0278-4343\(92\)90059-S](https://doi.org/10.1016/0278-4343(92)90059-S)
- Beardall, J., & Raven, J. A. (2013). Calcification and ocean acidification: New insights from the coccolithophore *Emiliana huxleyi*. *New Phytologist*, *199*, 1, 3. <https://doi.org/10.1111/nph.12297>
- Bidigare, R. R., Fluegge, A., Freeman, K. H., Hanson, K. L., Hayes, J. M., Hollander, D., et al. (1997). Consistent fractionation of ¹³C in nature and in the laboratory: Growth-rate effects in some haptophyte algae. *Global Biogeochemical Cycles*, *11*(2), 279–292. <https://doi.org/10.1029/96GB03939>
- Blanco-Ameijeiras, S., Stoll, H. M., Zhang, H., & Hopkinson, B. M. (2020). Influence of temperature and CO₂ on plasma-membrane permeability to CO₂ and HCO₃⁻ in the Marine Haptophytes *Emiliana huxleyi* and *Calcidiscus leptoporus* (Prymnesiophyceae). *Journal of Phycology*, *56*, 13017, 1294. <https://doi.org/10.1111/jpy.13017>
- Boller, A. J., Thomas, P. J., Cavanaugh, C. M., & Scott, K. M. (2011). Low stable carbon isotope fractionation by coccolithophore Rubisco. *Geochimica et Cosmochimica Acta*, *75*(22), 7200–7207. <https://doi.org/10.1016/j.gca.2011.08.031>
- Boller, A. J., Thomas, P. J., Cavanaugh, C. M., & Scott, K. M. (2015). Isotopic discrimination and kinetic parameters of RubisCO from the marine bloom-forming diatom, *Skeletonema costatum*. *Geobiology*, *13*(1), 33–43. <https://doi.org/10.1111/gbi.12112>

- Bolton, C. T., Hernández-Sánchez, M. T., Fuertes, M.-Á., González-Lemos, S., Abrevaya, L., Mendez-Vicente, A., et al. (2016). Decrease in coccolithophore calcification and CO₂ since the middle Miocene. *Nature Communications*, 7(1), 10284. <https://doi.org/10.1038/ncomms10284>
- Bolton, C. T., & Stoll, H. M. (2013). Late Miocene threshold response of marine algae to carbon dioxide limitation. *Nature*, 500(7464), 558–562. <https://doi.org/10.1038/nature12448>
- Brassell, S. C., & Dumitrescu, M. (2004). Recognition of alkenones in a lower Aptian porcellanite from the west-central Pacific. *Organic Geochemistry*, 35(2), 181–188. <https://doi.org/10.1016/j.orggeochem.2003.09.003>
- Burkhardt, S., Riebesell, U., & Zondervan, I. (1999). Effects of growth rate, CO₂ concentration, and cell size on the stable carbon isotope fractionation in marine phytoplankton. *Geochimica et Cosmochimica Acta*, 63(22), 3729–3741. [https://doi.org/10.1016/S0016-7037\(99\)00217-3](https://doi.org/10.1016/S0016-7037(99)00217-3)
- Burky, D. (1971). Cenozoic calcareous nannofossils from the Pacific Ocean. *Transactions of the San Diego Society of Natural History*, 16(14), 303–328.
- Dickson, A. G., Sabine, C. L., & Christian, J. R. (2007). *Guide to best practices for ocean CO₂ measurements*. North Pacific Marine Science Organization.
- Falkowski, P. G., & Raven, J. A. (2007). *Aquatic photosynthesis* (2nd ed.). Princeton University Press.
- Farquhar, G. D., O'Leary, M. H., & Berry, J. A. (1982). On the relationship between carbon isotope discrimination and the intercellular carbon dioxide concentration in leaves. *Functional Plant Biology*, 9(2), 121. <https://doi.org/10.1071/PP9820121>
- Faucher, G., Hoffmann, L., Bach, L. T., Bottini, C., Erba, E., & Riebesell, U. (2017). Impact of trace metal concentrations on coccolithophore growth and morphology: Laboratory simulations of Cretaceous stress. *Biogeosciences*, 14(14), 3603–3613. <https://doi.org/10.5194/bg-14-3603-2017>
- Francois, R., Altabet, M. A., Goericke, R., McCorkle, D. C., Brunet, C., & Poisson, A. (1993). Changes in the δ¹³C of surface water particulate organic matter across the subtropical convergence in the SW Indian Ocean. *Global Biogeochemical Cycles*, 7(3), 627, 644. <https://doi.org/10.1029/93GB01277>
- Freeman, K. H., & Hayes, J. M. (1992). Fractionation of carbon isotopes by phytoplankton and estimates of ancient CO₂ levels. *Global Biogeochemical Cycles*, 6(2), 185–198. <https://doi.org/10.1029/92gb00190>
- Freeman, K. H., & Pagani, M. (2005). Alkenone-based estimates of past CO₂ levels: A consideration of their utility based on an analysis of uncertainties. In *A History of Atmospheric CO₂ and Its Effects on Plants, Animals, and Ecosystems* (pp. 35–61). Springer.
- Gartner, S. (1969). Correlation of Neogene planktonic foraminifer and calcareous nannofossil zones.; Geology of the American Mediterranean. *Transactions - Gulf Coast Association of Geological Societies*, 19(March), 585–599. <https://doi.org/10.1306/a1adf339-0dfe-11d7-8641000102c1865d>
- Geitzenauer, K. R., Roche, M. B., & McIntyre, A. (1976). Modern pacific coccolith assemblages: Derivation and application to late Pleistocene paleotemperature analysis. *Memoir of the Geological Society of America*, 145, 423–448. <https://doi.org/10.1130/MEM145-p423>
- Goericke, R., Montoya, J. P., & Fry, B. (1994). Physiology of isotopic fractionation in algae and cyanobacteria. In K. Lajtha, & R. H. Michener (Eds.), *Stable Isotopes in Ecology and Environmental Science* (pp. 187–221). Blackwell Scientific Publications.
- Guillard, R. R. L., & Hargraves, P. E. (1993). *Stichochrysis immobilis* is a diatom, not a chrysophyte. *Phycologia*, 32(3), 234–236. <https://doi.org/10.2216/i0031-8884-32-3-234.1>
- Hagino, K., & Young, J. R. (2015). Biology and paleontology of Coccolithophores (Haptophytes). In S. Ohtsuka, T. Suzuki, T. Horiguchi, N. Suzuki, & F. Not (Eds.), *Marine Protists: Diversity and Dynamics* (pp. 311–330). Springer Japan. <https://doi.org/10.1007/978-4-431-55130-0>
- Henderiks, J., & Pagani, M. (2007). Refining ancient carbon dioxide estimates: Significance of coccolithophore cell size for alkenone-based pCO₂ records. *Paleoceanography*, 22(3). <https://doi.org/10.1029/2006PA001399>
- Henderiks, J., & Pagani, M. (2008). Coccolithophore cell size and the Paleogene decline in atmospheric CO₂. *Earth and Planetary Science Letters*, 269(3–4), 575–584. <https://doi.org/10.1016/j.epsl.2008.03.016>
- Hennon, G. M. M., Williamson, O. M., Hernández Limón, M. D., Haley, S. T., & Dyhrman, S. T. (2019). Non-linear physiology and gene expression responses of harmful Alga *Heterosigma akashiwo* to Rising CO₂. *Protist*, 170(1), 38–51. <https://doi.org/10.1016/j.protis.2018.10.002>
- Herrmann, S., & Thierstein, H. R. (2012). Cenozoic coccolith size changes—Evolutionary and/or ecological controls? *Palaeogeography, Palaeoclimatology, Palaeoecology*, 333–334, 92–106. <https://doi.org/10.1016/j.palaeo.2012.03.011>
- Heureux, A. M. C., Young, J. N., Whitney, S. M., Eason-Hubbard, M. R., Lee, R. B. Y., Sharwood, R. E., & Rickaby, R. E. M. (2017). The role of Rubisco kinetics and pyrenoid morphology in shaping the CCM of haptophyte microalgae. *Journal of Experimental Botany*, 68(14), 3959–3969. <https://doi.org/10.1093/jxb/erx179>
- Holtz, L.-M., Wolf-Gladrow, D., & Thoms, S. (2015). Numerical cell model investigating cellular carbon fluxes in *Emiliania huxleyi*. *Journal of Theoretical Biology*, 364, 305–315. <https://doi.org/10.1016/j.jtbi.2014.08.040>
- Holtz, L.-M., Wolf-Gladrow, D., & Thoms, S. (2017). Stable carbon isotope signals in particulate organic and inorganic carbon of coccolithophores – A numerical model study for *Emiliania huxleyi*. *Journal of Theoretical Biology*, 420(June 2016), 117–127. <https://doi.org/10.1016/j.jtbi.2017.01.030>
- Hopkinson, B. M. (2014). A chloroplast pump model for the CO₂ concentrating mechanism in the diatom *Phaeodactylum tricornutum*. *Photosynthesis Research*, 121(2–3), 223–233. <https://doi.org/10.1007/s11120-013-9954-7>
- Hopkinson, B. M., Dupont, C. L., Allen, A. E., & Morel, F. M. M. (2011). Efficiency of the CO₂-concentrating mechanism of diatoms. *Proceedings of the National Academy of Sciences*, 1, 3830–3837. <https://doi.org/10.1073/pnas.1018062108>
- Isensee, K., Erez, J., & Stoll, H. M. (2014). Detection of a variable intracellular acid-labile carbon pool in *Thalassiosira weissflogii* (Heterokontophyta) and *Emiliania huxleyi* (Haptophyta) in response to changes in the seawater carbon system. *Physiologia Plantarum*, 150(2), 321–338. <https://doi.org/10.1111/ppi.12096>
- Jasper, J. P., & Hayes, J. M. (1990). A carbon isotope record of CO₂ levels during the late Quaternary. *Nature*, 347(6292), 462–464. <https://doi.org/10.1038/347462a0>
- Jasper, J. P., Hayes, J. M., Mix, A. C., & Prah, F. G. (1994). Photosynthetic fractionation of ¹³C and concentrations of dissolved CO₂ in the central equatorial Pacific during the last 255,000 years. *Paleoceanography*, 9(6), 781–798. <https://doi.org/10.1029/94pa02116>
- Juhl, A. R., & Latz, M. I. (2002). Mechanisms of fluid shear-induced inhibition of population growth in a red-tide dinoflagellate. *Journal of Phycology*, 38(4), 683–694. <https://doi.org/10.1046/j.1529-8817.2002.00165.x>
- Keller, K., & Morel, F. M. M. (1999). A model of carbon isotopic fractionation and active carbon uptake in phytoplankton. *Marine Ecology Progress Series*, 182, 295–298. <https://doi.org/10.3354/meps182295>
- Ko, T. W., Lee, K. E., Bae, S. W., & Lee, S. (2018). Spatial and temporal distribution of C37 alkenones in suspended materials in the northern East China Sea. *Palaeogeography, Palaeoclimatology, Palaeoecology*, 493(January), 102–110. <https://doi.org/10.1016/j.palaeo.2018.01.004>

- Krumhardt, K. M., Lovenduski, N. S., Iglesias-Rodriguez, M. D., & Kleypas, J. A. (2017). Coccolithophore growth and calcification in a changing ocean. *Progress in Oceanography*, 159(October), 276–295. <https://doi.org/10.1016/j.pocean.2017.10.007>
- Laws, E. A. (1997). *Mathematical methods for Oceanographers: An introduction*. Wiley.
- Laws, E. A., & Bannister, T. T. (1980). Nutrient- and light-limited growth of *Thalassiosira fluviatilis* in continuous culture with implications for phytoplankton growth in the ocean. *Limnology & Oceanography*, 25(3), 457–473. <https://doi.org/10.4319/lo.2004.49.6.2316>
- Laws, E. A., Bidigare, R. R., & Popp, B. N. (1997). Effect of growth rate and CO₂ concentration on carbon isotopic fractionation by the marine diatom *Phaeodactylum tricornutum*. *Limnology & Oceanography*, 42(7), 1552–1560. <https://doi.org/10.4319/lo.1997.42.7.1552>
- Laws, E. A., Popp, B. N., Bidigare, R. R., Kennicutt, M. C., & Macko, S. A. (1995). Dependence of phytoplankton carbon isotopic composition on growth rate and [CO₂]aq: Theoretical considerations and experimental results. *Geochimica et Cosmochimica Acta*, 59(6), 1131–1138. [https://doi.org/10.1016/0016-7037\(95\)00030-4](https://doi.org/10.1016/0016-7037(95)00030-4)
- Laws, E. A., Popp, B. N., Cassar, N., & Tanimoto, J. (2002). ¹³C discrimination patterns in oceanic phytoplankton: Likely influence of CO₂ concentrating mechanisms, and implications for palaeoreconstructions. *Functional Plant Biology*, 29(3), 323. <https://doi.org/10.1071/FP01183>
- Lee, K. E., Lee, S., Park, Y., Lee, H. J., & Harada, N. (2014). Alkenone production in the East Sea/Japan Sea. *Continental Shelf Research*, 74, 1–10. <https://doi.org/10.1016/j.csr.2013.12.003>
- Lee, K. E., & Schneider, R. (2005). Alkenone production in the upper 200 m of the Pacific Ocean. *Deep-Sea Research Part I Oceanographic Research Papers*, 52(3), 443–456. <https://doi.org/10.1016/j.dsr.2004.11.006>
- Lewis, E., & Wallace, D. (1998). CO₂SYS: Program developed for CO₂ system calculations (Vol. 105, p. 4735). Oak Ridge National Laboratory-Carbon Dioxide Information Analysis Center.
- Lorimer, G. H., & Mizioro, H. M. (1980). Carbamate formation on the ε-amino group of a Lysyl residue as the basis for the activation of ribulosebiphosphate carboxylase by carbon dioxide and magnesium(2+). *Biochemistry*, 19(23), 5321–5328. <https://doi.org/10.1021/bi00564a027>
- Lueker, T. J., Dickson, A. G., & Keeling, C. D. (2000). Ocean pCO₂ calculated from dissolved inorganic carbon, alkalinity, and equations for K₁ and K₂: Validation based on laboratory measurements of CO₂ in gas and seawater at equilibrium. *Marine Chemistry*, 70(1–3), 105–119. [https://doi.org/10.1016/S0304-4203\(00\)00022-0](https://doi.org/10.1016/S0304-4203(00)00022-0)
- Mackinder, L. C. M., Wheeler, G., Schroeder, D., von Dassow, P., Riebesell, U., & Brownlee, C. (2011). Expression of biomimetalization-related ion transport genes in *Emiliania huxleyi*. *Environmental Microbiology*, 13(12), 3250–3265. <https://doi.org/10.1111/j.1462-2920.2011.02561.x>
- Marlowe, I. T., Green, J. C., Neal, A. C., Brassell, S. C., Eglinton, G., & Course, P. A. (1984). Long chain (n-C37–C39) alkenones in the Prymnesiophyceae. Distribution of alkenones and other lipids and their taxonomic significance. *British Phycological Journal*, 19(3), 203–216. <https://doi.org/10.1080/00071618400650221>
- McClelland, H. L. O., Barbarin, N., Beaufort, L., Hermoso, M., Ferretti, P., Greaves, M., & Rickaby, R. E. M. (2016). Calcification response of a key phytoplankton family to millennial-scale environmental change. *Scientific Reports*, 6, 1–11. <https://doi.org/10.1038/srep34263>
- McClelland, H. L. O., Bruggeman, J., Hermoso, M., & Rickaby, R. E. M. (2017). The origin of carbon isotope vital effects in coccolith calcite. *Nature Communications*, 8(1), 14511. <https://doi.org/10.1038/ncomms14511>
- McIntyre, A., & Bé, A. W. H. (2003). Modern coccolithophoridae of the atlantic ocean—I. Placoliths and cyrtoliths. *Deep Sea Research and Oceanographic Abstracts*, 14(5), 561–597. [https://doi.org/10.1016/0011-7471\(67\)90065-4](https://doi.org/10.1016/0011-7471(67)90065-4)
- Montagnes, D. J. S., Berges, J. A., Harrison, P. J., & Taylor, F. J. R. (1993). Estimating carbon, nitrogen, protein, and chlorophyll a from volume in marine phytoplankton. *Limnology & Oceanography*, 39(5), 1044–1060.
- Moolna, A., & Rickaby, R. E. M. (2012). Interaction of the coccolithophore *Gephyrocapsa oceanica* with its carbon environment: Response to a recreated high-CO₂ geological past. *Geobiology*, 10(1), 72–81. <https://doi.org/10.1111/j.1472-4669.2011.00308.x>
- Müller, M. N., Antia, A. N., & LaRoche, J. (2008). Influence of cell cycle phase on calcification in the coccolithophore *Emiliania huxleyi*. *Limnology & Oceanography*, 53(2), 506–512. <https://doi.org/10.4319/lo.2008.53.2.0506>
- O’Leary, M. H. (1984). Measurement of the isotope fractionation associated with diffusion of carbon dioxide in aqueous solution. *The Journal of Physical Chemistry*, 88(4), 823–825. <https://doi.org/10.1021/j150648a041>
- Olsen, A., Key, R. M., Van Heuven, S., Lauvset, S. K., Velo, A., Lin, X., et al. (2016). The global ocean data analysis project version 2 (GLODAPv2) - An internally consistent data product for the world ocean. *Earth System Science Data*, 8(2), 297–323. <https://doi.org/10.5194/essd-8-297-2016>
- Pagani, M. (2014). Biomarker-based inferences of past climate: The alkenone pCO₂ proxy. In *Treatise on Geochemistry* (2nd ed., Vol. 12, pp. 361–378). Elsevier. <https://doi.org/10.1016/B978-0-08-095975-7.01027-5>
- Pagani, M., Arthur, M. A., & Freeman, K. H. (1999). Miocene evolution of atmospheric carbon dioxide. *Paleoceanography*, 14(3), 273–292. <https://doi.org/10.1029/1999PA900006>
- Pagani, M., Arthur, M. A., & Freeman, K. H. (2000). Variations in Miocene phytoplankton growth rates in the southwest Atlantic: Evidence for changes in ocean circulation. *Paleoceanography*, 15(5), 486–496. <https://doi.org/10.1029/1999PA000484>
- Pagani, M., Freeman, K. H., Ohkouchi, N., & Caldeira, K. (2002). Comparison of water column [CO₂aq] with sedimentary alkenone-based estimates: A test of the alkenone-CO₂ proxy. *Paleoceanography*, 17(4), 21–12112. <https://doi.org/10.1029/2002PA000756>
- Pagani, M., Huber, M., Liu, Z., Bohaty, S. M., Henderiks, J., Sijp, W., et al. (2011). The role of carbon dioxide during the onset of Antarctic Glaciation. *Science*, 334(6060), 1261–1264. <https://doi.org/10.1126/science.1203909>
- Pagani, M., Liu, Z., LaRiviere, J., & Ravelo, A. C. (2010). High Earth-system climate sensitivity determined from Pliocene carbon dioxide concentrations - Supplement. *Nature Geoscience*, 3(1), 27–30. <https://doi.org/10.1038/ngeo724>
- Pagani, M., Zachos, J. C., Freeman, K. H., Tipple, B., & Bohaty, S. (2005). Marked decline in atmospheric carbon dioxide concentrations during the paleogene. *Science*, 309(5734), 600–603. <https://doi.org/10.1126/science.1110063>
- Polissar, P. J., & D’Andrea, W. J. (2014). Uncertainty in paleohydrologic reconstructions from molecular δD values. *Geochimica et Cosmochimica Acta*, 129, 146–156. <https://doi.org/10.1016/j.gca.2013.12.021>
- Popp, B. N., Kenig, F., Wakeham, S. G., Laws, E. A., & Bidigare, R. R. (1998a). Does growth rate affect ketone unsaturation and intracellular carbon isotopic variability in *Emiliania huxleyi*? *Paleoceanography*, 13(1), 35–41. <https://doi.org/10.1029/97PA02594>
- Popp, B. N., Laws, E. A., Bidigare, R. R., Dore, J. E., Hanson, K. L., & Wakeham, S. G. (1998b). Effect of phytoplankton cell geometry on carbon isotopic fractionation. *Geochimica et Cosmochimica Acta*, 62(1), 69–77. [https://doi.org/10.1016/S0016-7037\(97\)00333-5](https://doi.org/10.1016/S0016-7037(97)00333-5)
- Popp, B. N., Prahl, F. G., Wallsgrove, R. J., & Tanimoto, J. (2006). Seasonal patterns of alkenone production in the subtropical oligotrophic North Pacific. *Paleoceanography*, 21(1), PA1004. <https://doi.org/10.1029/2005PA001165>
- Popp, B. N., Takigiku, R., Hayes, J. M., Louda, J., & Baker, E. W. (1989). The post-paleozoic chronology and mechanism of ¹³C depletion in primary marine organic matter. *American Journal of Science*, 289, 436–454. <https://doi.org/10.2475/ajs.289.4.436>

- Quiroga, O., & González, E. L. (1993). Carbonic anhydrase in the chloroplast of a coccolithophorid (Prynesiophyceae). *Journal of Phycology*, 29(3), 321–324. <https://doi.org/10.1111/j.0022-3646.1993.00321.x>
- Rau, G. H., Chavez, F. P., & Friederich, G. E. (2001). Plankton $^{13}\text{C}/^{12}\text{C}$ variations in Monterey Bay, California: Evidence of non-diffusive inorganic carbon uptake by phytoplankton in an upwelling environment. *Deep-Sea Research Part I Oceanographic Research Papers*, 48(1), 79–94. [https://doi.org/10.1016/S0967-0637\(00\)00039-X](https://doi.org/10.1016/S0967-0637(00)00039-X)
- Rau, G. H., Riebesell, U., & Wolf-Gladrow, D. (1996). A model of photosynthetic ^{13}C fractionation by marine phytoplankton based on diffusive molecular CO_2 uptake. *Marine Ecology Progress Series*, 133, 275–285. <https://doi.org/10.3354/meps133275>
- Rau, G. H., Takahashi, T., & Des Marais, D. J. (1989). Latitudinal variations in plankton $\delta^{13}\text{C}$: Implications for CO_2 and productivity in past oceans. *Nature*, 341(6242), 516–518. <https://doi.org/10.1038/341516a0>
- Rau, G. H., Takahashi, T., Desmarais, D. J., Repeta, D. J., & Martin, J. H. (1992). The relationship between d^{13}C of organic-matter and $[\text{CO}_2(\text{aq})]$ in ocean surface-water: Data from a JGOFS site in the Northeast Atlantic-Ocean and a model. *Geochimica et Cosmochimica Acta*, 56, 1413–1419. [https://doi.org/10.1016/0016-7037\(92\)90073-R](https://doi.org/10.1016/0016-7037(92)90073-R)
- Raven, J. A. (1997). Inorganic carbon acquisition by marine autotrophs. In *Advances in Botanical Research*, 27, 85–209. [https://doi.org/10.1016/s0065-2296\(08\)60281-5](https://doi.org/10.1016/s0065-2296(08)60281-5)
- Rickaby, R. E. M., Henderiks, J., & Young, J. N. (2010). Perturbing phytoplankton: Response and isotopic fractionation with changing carbonate chemistry in two coccolithophore species. *Climate of the Past*, 6(6), 771–785. <https://doi.org/10.5194/cp-6-771-2010>
- Riebesell, U., Burkhardt, S., Dauelsberg, A., & Kroon, B. (2000a). Carbon isotope fractionation by a marine diatom: Dependence on the growth-rate-limiting resource. *Marine Ecology Progress Series*, 193, 295–303. <https://doi.org/10.3354/meps193295>
- Riebesell, U., Revill, A. T., Holdsworth, D. G., & Volkman, J. K. (2000b). The effects of varying CO_2 concentration on lipid composition and carbon isotope fractionation in *Emiliania huxleyi*. *Geochimica et Cosmochimica Acta*, 64(24), 4179–4192. [https://doi.org/10.1016/S0016-7037\(00\)00474-9](https://doi.org/10.1016/S0016-7037(00)00474-9)
- Riebesell, U., & Wolf-Gladrow, D. A. (1995). Growth limits on Phytoplankton. *Nature*, 373(5), 28. <https://doi.org/10.1038/373028b0>
- Roeske, C. A., & O'Leary, M. H. (1985). Carbon isotope effect on carboxylation of ribulose biphosphate catalyzed by ribulose biphosphate carboxylase from *Rhodospirillum rubrum*. *Biochemistry*, 24(7), 1603–1607. <https://doi.org/10.1021/bi00328a005>
- Rost, B., Riebesell, U., Burkhardt, S., & Sültemeyer, D. (2003). Carbon acquisition of bloom-forming marine phytoplankton. *Limnology & Oceanography*, 48(1), 55–67. <https://doi.org/10.4319/lo.2003.48.1.0055>
- Rost, B., Riebesell, U., & Sültemeyer, D. (2006). Carbon acquisition of marine phytoplankton: Effect of photoperiod length. *Limnology & Oceanography*, 51(1), 12–20. <https://doi.org/10.4319/lo.2006.51.1.0012>
- Rost, B., Zondervan, I., & Riebesell, U. (2002). Light-dependent carbon isotope fractionation in the coccolithophorid *Emiliania huxleyi*. *Limnology & Oceanography*, 47(1), 120–128. <https://doi.org/10.4319/lo.2002.47.1.0120>
- Schouten, S., Ossebaar, J., Schreiber, K., Kienhuis, M. V. M., Langer, G., Benthien, A., & Bijma, J. (2006). The effect of temperature, salinity and growth rate on the stable hydrogen isotopic composition of long chain alkenones produced by *Emiliania huxleyi* and *Gephyrocapsa oceanica*. *Biogeosciences*, 3(1), 113–119. <https://doi.org/10.5194/bg-3-113-2006>
- Sett, S., Bach, L. T., Schulz, K. G., Koch-Klavens, S., Lebrato, M., & Riebesell, U. (2014). Temperature modulates Coccolithophorid sensitivity of growth, photosynthesis and calcification to increasing seawater pCO_2 . *PLoS One*, 9(2), e88308. <https://doi.org/10.1371/journal.pone.0088308>
- Stojkovic, S., Beardall, J., & Matear, R. (2013). CO_2 -concentrating mechanisms in three southern hemisphere strains of *Emiliania huxleyi*. *Journal of Phycology*, 49(4), 670–679. <https://doi.org/10.1111/jpy.12074>
- Stoll, H. M., Guitian, J., Hernandez-Almeida, I., Mejia, L. M., Phelps, S. R., Polissar, P. J., et al. (2019). Upregulation of phytoplankton carbon concentrating mechanisms during low CO_2 glacial periods and implications for the phytoplankton pCO_2 proxy. *Quaternary Science Reviews*, 208, 1–20. <https://doi.org/10.1016/j.quascirev.2019.01.012>
- Thompson, P. A., & Calvert, S. E. (1995). Carbon isotope fractionation by *Emiliania huxleyi*. *Limnology & Oceanography*, 40(4), 673–679. <https://doi.org/10.4319/lo.1995.40.4.0673>
- Uppström, L. R. (1974). The boron/chlorinity ratio of deep-sea water from the Pacific Ocean. *Deep Sea Research and Oceanographic Abstracts*, 21(2), 161–162. [https://doi.org/10.1016/0011-7471\(74\)90074-6](https://doi.org/10.1016/0011-7471(74)90074-6)
- van der Meer, M. T. J., Benthien, A., French, K. L., Epping, E., Zondervan, I., Reichart, G. J., et al. (2015). Large effect of irradiance on hydrogen isotope fractionation of alkenones in *Emiliania huxleyi*. *Geochimica et Cosmochimica Acta*, 160, 16–24. <https://doi.org/10.1016/j.gca.2015.03.024>
- Verity, P. G., Robertson, C. Y., Tronzo, C. R., Andrews, M. G., Nelson, J. R., & Sieracki, M. E. (1992). Relationships between cell volume and the carbon and nitrogen content of marine photosynthetic nanoplankton. *Limnology & Oceanography*, 37(7), 1434–1446. <https://doi.org/10.4319/lo.1992.37.7.1434>
- Weiss, G. M., Roepert, A., Middelburg, J. J., Schouten, S., Sinninghe Damsté, J. S., & van der Meer, M. T. J. (2019). Hydrogen isotope fractionation response to salinity and alkalinity in a calcifying strain of *Emiliania huxleyi*. *Organic Geochemistry*, 134, 62–65. <https://doi.org/10.1016/j.orggeochem.2019.06.001>
- Wilkes, E. B., Lee, R. B. Y., McClelland, H. L. O., Rickaby, R. E. M., & Pearson, A. (2018). Carbon isotope ratios of coccolith-associated polysaccharides of *Emiliania huxleyi* as a function of growth rate and CO_2 concentration. *Organic Geochemistry*, 119, 1–10. <https://doi.org/10.1016/j.orggeochem.2018.02.006>
- Wilkes, E. B., & Pearson, A. (2019). A general model for carbon isotopes in red-lineage phytoplankton: Interplay between unidirectional processes and fractionation by RubisCO. *Geochimica et Cosmochimica Acta*, 265, 163–181. <https://doi.org/10.1016/j.gca.2019.08.043>
- Wolhowe, M. D., Prah, F. G., Langer, G., Oviedo, A. M., & Ziveri, P. (2015). Alkenone δD as an ecological indicator: A culture and field study of physiologically-controlled chemical and hydrogen-isotopic variation in C37 alkenones. *Geochimica et Cosmochimica Acta*, 162, 166–182. <https://doi.org/10.1016/j.gca.2015.04.034>
- Wolhowe, M. D., Prah, F. G., White, A. E., Popp, B. N., & Rosas-Navarro, A. (2014). A biomarker perspective on coccolithophorid growth and export in a stratified sea. *Progress in Oceanography*, 122, 65–76. <https://doi.org/10.1016/j.pocan.2013.12.001>
- Young, J. N. (2011). *Past and future adaptations of phytoplankton to carbon dioxide*. Oxford University.
- Young, J. N., Heureux, A. M. C., Sharwood, R. E., Rickaby, R. E. M., Morel, F. M. M., & Whitney, S. M. (2016). Large variation in the Rubisco kinetics of diatoms reveals diversity among their carbon-concentrating mechanisms. *Journal of Experimental Botany*, 67(11), 3445–3456. <https://doi.org/10.1093/jxb/erw163>
- Young, J. N., Rickaby, R. E. M., Kapralov, M. V., & Filatov, D. A. (2012). Adaptive signals in algal RuBisCO reveal a history of ancient atmospheric carbon dioxide. *Philosophical Transactions of the Royal Society B: Biological Sciences*, 367(1588), 483–492. <https://doi.org/10.1098/rstb.2011.0145>

- Young, J. R., Geisen, M., Cros, L., Kleijne, A., Sprengel, C., Probert, I., & Østergaard, J. (2003). A guide to extant coccolithophore taxonomy. *Journal of Nannoplankton Research*, Special Issue 1, 125.
- Zeebe, R. E., Ridgwell, A. J., & Zachos, J. C. (2016). Anthropogenic carbon release rate unprecedented during the past 66 million years. *Nature Geoscience*, 9(4), 325–329. <https://doi.org/10.1038/ngeo2681>
- Zeebe, R. E., & Wolf-Gladrow, D. A. (2001). *CO₂ in seawater: Equilibrium, kinetics* (1st ed., Vol. 65). Elsevier. [https://doi.org/10.1016/S0924-7963\(02\)00179-3](https://doi.org/10.1016/S0924-7963(02)00179-3)
- Zhang, Y. G., Henderiks, J., & Liu, X. (2020). Refining the alkenone-pCO₂ method II: Toward resolving the physiological parameter 'b'. *Geochimica et Cosmochimica Acta*, 281, 118–134. <https://doi.org/10.1016/j.gca.2020.05.002>
- Zhang, Y. G., Pagani, M., Henderiks, J., & Ren, H. (2017). A long history of equatorial deep-water upwelling in the Pacific Ocean. *Earth and Planetary Science Letters*, 467, 1–9. <https://doi.org/10.1016/j.epsl.2017.03.016>
- Zhang, Y. G., Pagani, M., Liu, Z., Bohaty, S. M., & DeConto, R. (2013). A 40-million-year history of atmospheric CO₂. *Philosophical Transactions of the Royal Society A: Mathematical, Physical & Engineering Sciences*, 371, 20130096. <https://doi.org/10.1098/rsta.2013.0096>
- Zhang, Y. G., Pearson, A., Benthien, A., Dong, L., Huybers, P., Liu, X., & Pagani, M. (2019). Refining the alkenone-pCO₂ method I: Lessons from the quaternary glacial cycles. *Geochimica et Cosmochimica Acta*, 260, 177–191. <https://doi.org/10.1016/j.gca.2019.06.032>